UTM
UNIVERSITI TEKNOLOGI MALAYSIA

UTM Razak School of Engineering and Advanced Technology

Proceedings of the 1st Master Project Symposium on Systems Engineering and Professional Science

Editors:
Dr. Siti Zura A. Jalil @ Zainuddin
Dr. Sharifah Alwiah Syed Abd. Rahman
Dr. Rahimah Muhamad
Dr. Mohd Nabil Muhtazaruddin

utmrazakschool.utm.my

PROCEEDINGS OF THE 1st MASTER PROJECT SYMPOSIUM ON SYSTEMS ENGINEERING AND PROFESSIONAL SCIENCE

13 – 15th DECEMBER 2016
UNIVERSITI TEKNOLOGI MALAYSIA
KUALA LUMPUR

ISBN: 978-967-13383-5-3

Published by:
UTM Razak School of Engineering and Advanced Technology
Universiti Teknologi Malaysia
Level 7, Razak Tower
Jalan Sultan Yahya Petra
54100 Kuala Lumpur
MALAYSIA
http://razakschool.utm.my

First Printing, April 2017
Printed in Malaysia

Editors:

Dr. Siti Zura A. Jalil @ Zainuddin
Dr. Sharifah Alwiah Syed Abd. Rahman
Dr. Rahimah Muhamad
Dr. Mohd Nabil Muhtazaruddin

Associate Editors:

Dr. Fatimah Salim
Dr. Hayati @ Habibah Abdul Talib
Dr. Nor Raihana Mohd Ali
Dr. Habibah @ Norehan Hj. Haron
Dr. Roslina Mohammad
Dr. Samira Albati Kamaruddin
Dr. Shamsul Sarip
Dr. Sa'ardin Abdul Aziz
Dr. Siti Armiza Mohd Aris

About Master Project Symposium

The 1st Master Project Symposium was held on 13-15 December 2016 for Semester 1 Session 2016/2017 at Menara Razak, Universiti Teknologi Malaysia (UTM) Kuala Lumpur. This symposium is organized every semester by Master Project Committee, UTM Razak School of Engineering and Advanced Technology to fulfil the requirement of Master of Science (Systems Engineering) and Master of Professional Science.

This symposium aims to provide a platform for students to share their research processes and outcomes among UTM Razak School members and at the same time receive inputs from the audience to improve their research. Students are exposed to various systems engineering and professional science by identifying the current issues in their workplaces and addressing the issue through their research.

The papers presented in the symposium are compiled into proceedings to share the research conducted by the students and findings that relates to the current practices of many of the industries in Malaysia. An index of keywords from all papers is included at the end of the proceedings. All participants and readers can enjoy reading the proceedings and gain inspirations for further research and application into education and practice.

Contents

A New Power Consumption Model for Virtual Machines Placement in Cloud Data Center

Mohd Zain Hassan[a], Rudzidatul Akmam Dziyauddin[b] and Hazilah Mad Kaidi[c]

UTM Razak School of Engineering and Advanced Technology, Universiti Teknologi Malaysia, Jalan Sultan Yahya Petra, 53100 Kuala Lumpur, Malaysia

[a]*mzainh@gmail.com,* [b]*rudzidatul.kl@utm.my,* [c]*hazilah.kl@utm.my*

Abstract – *As business relies on Information Technology (IT) in driving business goals, a computer resource demand has been dramatically increased, and it introduces several challenges to IT service providers. Virtualization is a technique that can be used to reduce hardware footprint and thus realizing power efficiency. However, improper placement technique has caused many cloud servers being provisioned inefficiently. Consequently, many physical servers installed as hypervisors utilize high power in data center and simultaneously existing servers are underutilized. This study focuses on identifying a relationship between virtual central processing unit (CPU), physical CPU and power consumption. We developed a model to estimate power requirements for virtual machines (VM) in cloud data center. The model is applicable to steady-state cloud data centers or in systems engineering design phase. The model can also be extended in determining a cloud server charge back model subject to power consumption.*

Keywords: Virtualization, Power Consumption, Cloud computing, Hypervisor, VMware

1.0 INTRODUCTION

Information Technology (IT) is growing rapidly in a global scale. Nowadays, business strategy of companies is embedding information technology strategy in their business models [1] and thus making IT as one of the predominant factors in enabling business opportunities for organization. The demand of computing resources has been increased tremendously over the last few years due to this scenario [2]. The trend has directly resulting growth and increase the need for businesses to subscribe for IT service providers. The increased of demand has challenged IT service providers to establish large-scale data centers containing many different type of computing equipment to cater the needs.

The recent advances in IT has introduce many techniques in managing efficiency of servers in data centers. Some of the techniques include physical server consolidation, physical server virtualization [3], natural air cooling system, and software-defined computing resource management. Virtualization concept introduces energy efficiency, however there are lack standard in measuring virtual machine and host power efficiency in the datacentre [4]. This introduce challenges to understand the deep and complex interactions between performance of virtual systems with power management and how efficiency can be managed [5].

IT service providers are over-provisioning virtual machines in cloud data center assuming that they will achieve energy efficient by implementing virtualization [4]. However, this introduced a new problem when high energy are consumed when many of the servers are not fully utilized [6] and virtual machines placement are not balanced [7]. The main cause of this problem is due to lack of standard in estimating virtual machine energy consumption [4].

The aim of the research is to classify energy efficient hypervisor based on manufacturing standard. In this paper, a mathematical model is developed to estimate power consumption of hypervisor based on virtual servers' utilization. The model is then used together with the classification data from manufacturing standard to propose algorithm that will help the IT Service Providers in achieving energy efficiency in the cloud or virtualization systems based on the virtual server's utilization and power estimation model.

2.0 METHODOLOGY

2.1 Conceptual Framework

The research is designed to collect and analyse data based on the variables shown in Figure 1 below. Physical layers involves data from every hosts in the cloud data center farms in this research. There are 16 hosts configured for each of the farm. The power consumption and CPU utilization data are collected. In virtual layer, the data is taken by getting the CPU utilization reading in every virtual machines hosted in 16 hosts. There are total of 938 virtual machines involved during the data collection.

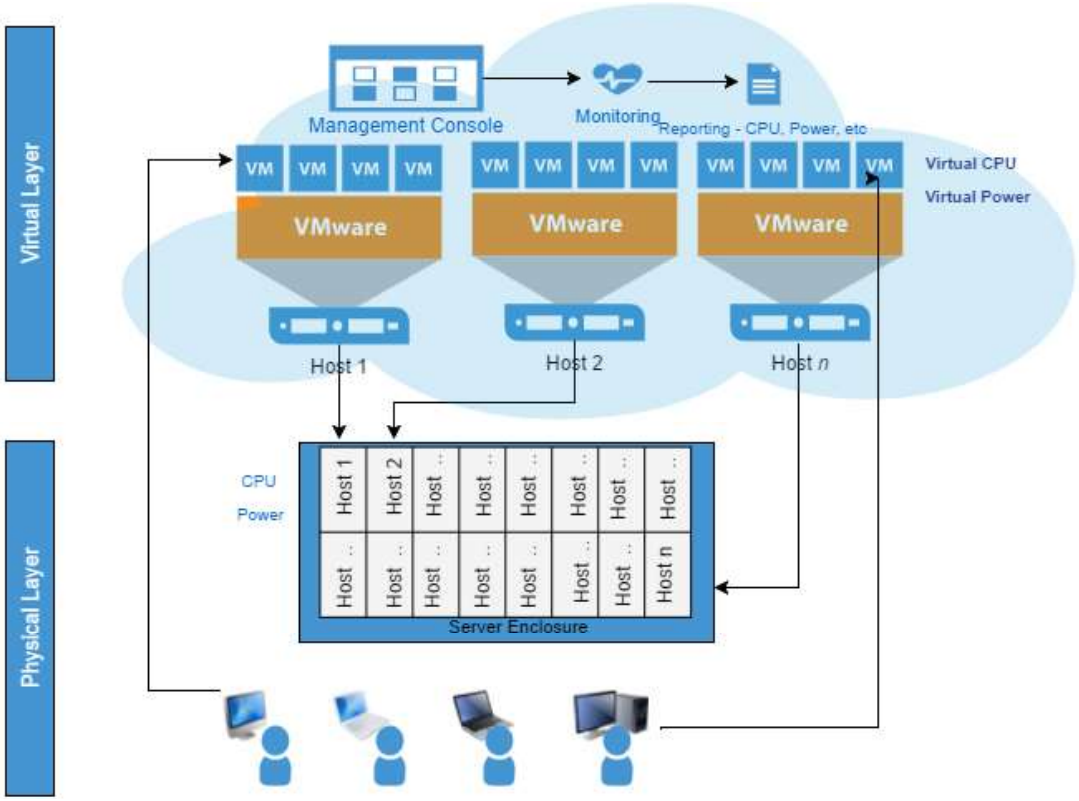

Figure 1: Conceptual Framework of the Study

A limitation of this study is that it only uses a single virtualization technology. Secondly, the study does not consider other external factors that might impact power utilization in the host server such as power surge, high disk I/O operations and memory usage. Thirdly, the power reading were collected from server power supply sensor but other performance data for CPU are collected via hypervisor software. The method could have a small timing inconsistency without affecting the data validity.

2.2 Data Center Efficiency and Power Model

Data center efficiency is measured using power usage effectiveness (PUE) indicator [8]. It is measured as ratio of IT load against the total facility load. The goal in data center efficiency is to reduce the PUE to the lowest possible value. The IT load is referring to power usage of IT equipment comprises of servers, network, storage devices and management hardware [9]. Since the study focus the relationship of virtual servers and its hypervisor CPU and power consumption, the scope of the work is to analyze server element and reduce the power consumption. The total server power is the summation of non-hypervisor and hypervisor server power. In the organization where this study is conducted, 90% of the workload is hosted by hypervisor servers. According to study [10]–[12], both energy consumption and CPU utilization have almost linear correlation between two machines. In spite of servers using Dynamic Voltage Frequency Scaling (DVFS), the study [10] reveals the energy-saving effect technique of DVFS is not so obvious and linear correlation can still predict the power consumption effectively. In this study, we are proposing a linear correlation of power model by taking virtual machines into account. It is also understood that Operating Systems of the server has kernel processes that utilizes certain amount of available CPU. Therefore, a power model in this study can be written as (1).

$$Hypervisor\ Power = \sum_{i=1}^{n} VMs\ virtual\ CPU + Hypervisor\ Kernel\ CPU\ usage \quad (1)$$

2.3 Data Analysis and Methodology

Several research questions have been developed to design data collection and analysis for this study. The data will be collected from one of a leading global IT Service Provider company based in the USA. Firstly, data of server utilization during idle and peak performance is gathered from server hardware manufacturer whitepaper to answer question of host minimum and maximum power consumption. Secondly, another important question is to understand the relationship between host CPU utilization and its power. The third question is to understand the relationship between virtual servers CPU usage and its hypervisor CPU. Both of the questions will be addressed by collecting performance data of 16 hypervisors and 937 virtual servers over a period of 5 days in every 20 seconds internal for one hour. All of the hypervisors in this study are using VMware, hence the performance data of CPU will be collected via PowerCLI software by connecting to vSphere server that is managing this infrastructure. A custom script is written to collect the data in the mentioned period. Hypervisor host power information is collected by running a custom script using PowerShell software. Since all of the servers in this research are using Hewlett Packard Enterprise Proliant hardware, a third party scripting tool called HPiLO

cmdlet from the hardware vendor is used with the PowerShell software to read power supply sensor directly from each of the server.

The data collection in this study using PowerShell and PowerCLI tool was set to run from a central location server that is located in the same data center of servers in study. This is to prevent potential network congestion which may cause an error during the collection. An automated job is set so the data can be collected simultaneously in the mentioned period. After five days, the data is extracted and combined using Microsoft Excel. The combined data is then analyzed using statistical software Minitab to get the required correlation and regression model.

3.0 RESULTS AND DISCUSSION

3.1 Relationship of Virtual Machine CPU, Host CPU and Host Power utilization

The study has collected the data from using the method and tools, which is explained in Section 2.3. The relationship of host CPU utilization and power consumption is illustrated in Figure 2. By using Pearson analysis, both variables are tested and the P-Value is determined as 0.01. Since the P-Value is low (less than 0.05), the study indicates that the correlation is statistically significant based on 95% significant level. A linear correlation in Figure 2 implies a fitted equation as in (2)

$$\text{Power utilization} = 194.6 + 0.0003766 \times \text{CPU usage} \quad (2)$$

Figure 2 yields that the host power utilization can be predicted from the CPU usage.

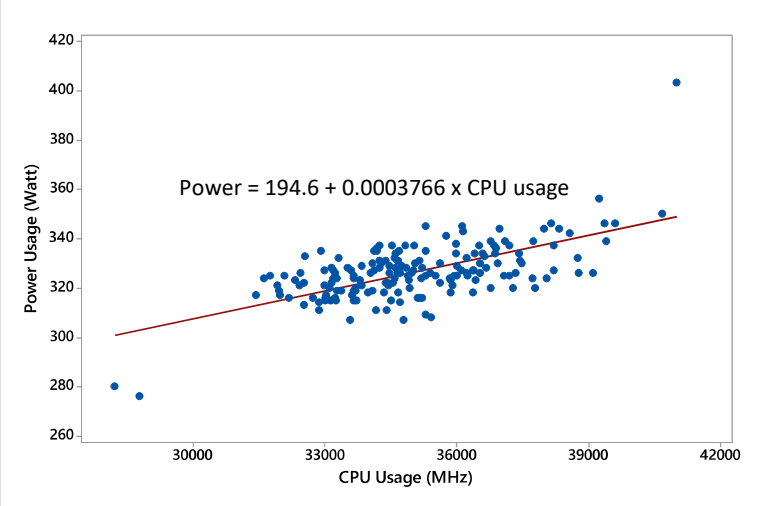

Figure 2: Analysis of Relationship between Hypervisor CPU and Power Utilization

The results are compared against a power model introduced by Beloglazov, 2013 [6]. The collected data is fitted into the power model in previous study. A comparison of the proposed power model and the previous power model [6] using a probability plot with 99% confidence level is shown in Figure 3. The figure demonstrates a clear linear pattern for both power models, which validates the proposed power model in this study. In essence, the proposed power model can be used to describe the relationship of CPU usage and power utilisation for hypervisors.

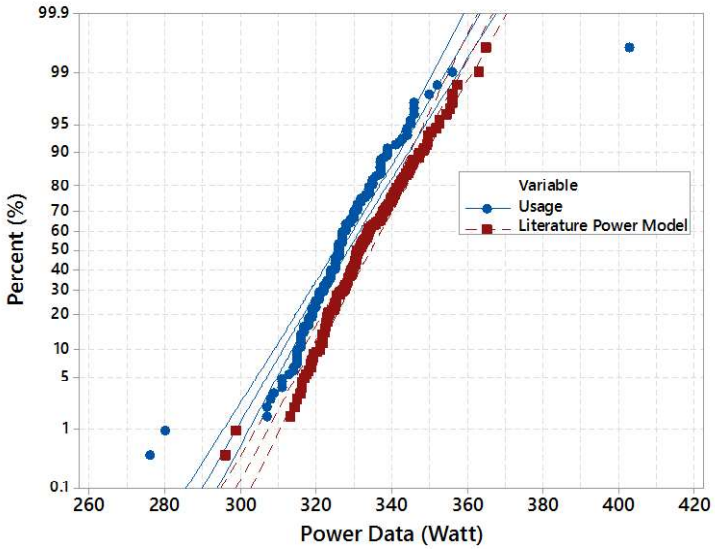

Figure 3: Power Model Relationship

In order to analyze the relationship between total virtual machines and host CPU usage, a linear regression analysis is performed. The results of the analysis are presented in Figure 4. It can be noted from the results that there is a significant positive relationship between total VM and host CPU usage. A third variable, host kernel processes is also explored and a regression model is developed with strong R-sq variation of 99.80%. The model is explained in (3).

$$\text{hCPU} = 1067 + 0.99267 * \sum_{i=1}^{n} vCPU + 1.0171 \ * kCPU \quad (3)$$

where *vCPU* is the total CPU usage of the virtual machines, and *kCPU* is the CPU utilization of the kernel processes in the host.

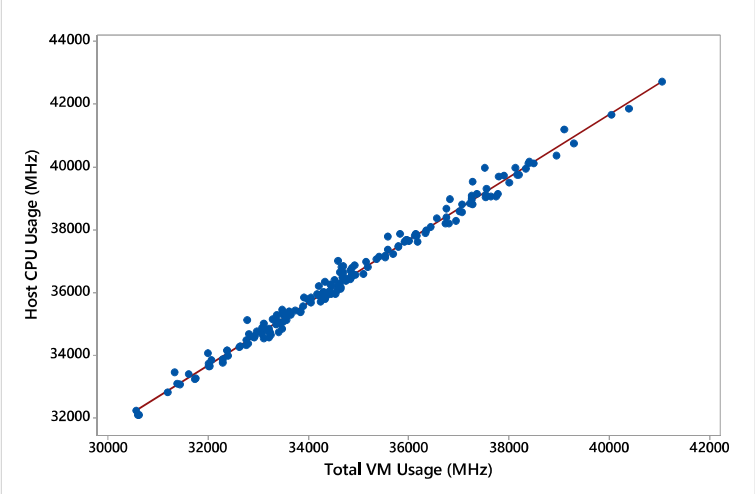

Figure 4: Total VM Usage and Host CPU Usage Relationship

4.0 CONCLUSION

This study was conducted to establish the relationship of virtual machines CPU usage to host CPU and its power consumption. The regression analysis has revealed that there is a significant relationship between the virtual machines CPU and host CPU usage. The relevance of this relationship was also supported by the regression analysis of host CPU usage to its power. Based on the results of the multi regression analysis, a simplified power model of the cloud data center farm was developed to predict the power consumption of a host. For future work, the power consumption model will be conceptually tested and the relationship of host CPU usage, host CPU and power consumption can be accessed by using machine learning.

REFERENCES

[1] A. Bharadwaj, O. a. El Sawy, P. a. Pavlou, and N. Venkatraman, "Digital Business Strategy: Toward a Next Generation of Insights," MIS Q., vol. 37, no. 2 (2013): 471–482.

[2] J. Subirats and J. Guitart, "Assessing and forecasting energy efficiency on Cloud computing platforms," Futur. Gener. Comput. Syst., vol. 45 (2015): pp. 70–94.

[3] A. F. Monteiro, M. V. Azevedo, and A. Sztajnberg, "Virtualized Web server cluster self-configuration to optimize resource and power use," J. Syst. Softw., vol. 86, no. 11 (2013): 2779–2796.

[4] M. Uddin and A. A. Rahman, "Energy efficiency and low carbon enabler green IT framework for data centers considering green metrics," Renew. Sustain. Energy Rev., vol. 16, no. 6 (2012) : 4078–4094.

[5] K. W. Cameron, "Energy efficiency in the wild: Why datacenters fear power management," Computer (Long. Beach. Calif)., vol. 47, no. 11, (2014): 89–92.

[6] A. Beloglazov, "Energy-Efficient Management of Virtual Machines in Data Centers for Cloud Computing," The University of Melbourne, (2013).

[7] X. Li, Z. Qian, S. Lu, and J. Wu, "Energy efficient virtual machine placement algorithm with balanced and improved resource utilization in a data center," Math. Comput. Model., vol. 58, no. 5–6 (2013) : 1222–1235.

[8] V. Avelar, D. Azevedo, and A. French, "PUE^{TM}: A Comprehensive Examination of the Metric," (2012) : 1–83.

[9] A. H. Beitelmal and D. Fabris, "Servers and data centers energy performance metrics," Energy Build., vol. 80 (2014) : 562–569.

[10] H. Rong, H. Zhang, S. Xiao, C. Li, and C. Hu, "Optimizing energy consumption for data centers," Renew. Sustain. Energy Rev., vol. 58 (2016) : 674–691.

[11] A. Beloglazov and R. Buyya, "OpenStack Neat: A framework for dynamic and energy-efficient consolidation of virtual machines in OpenStack clouds," Concurr. Comput., vol. 27, no. 5 (2015): 1310–1333.

[12] R. Buyya, A. Beloglazov, and J. Abawajy, "Energy-Efficient Management of Data Center Resources for Cloud Computing : A Vision , Architectural Elements , and Open Challenges Clou d Computing and D istributed S ystems (CLOUDS) Laboratory Department of Computer Science and Software Engineering The," Univ. Melbourne, Aust., no. Vm (2010): 1–12.

Analysis of Rainfall Distribution in Sabah Using Double Smoothing Method

Hazlina Ahmad[a], Norzaida Abas[b], Zalina Mohd. Daud[c] and Sharifah Alwiah Syed Abd. Rahman[d]

UTM RazakSchool of Engineering and Advanced Technology
Universiti Teknologi Malaysia Kuala Lumpur, 54100Kuala Lumpur, Malaysia

[a]*faziliena@yahoo.com,* [b]*zaida.kl@utm.my,* [c]*zalina.kl@utm.my,* [d]*shalwiah.kl@utm.my*

Abstract *–Time series analysis is an important tool in modelling and forecasting of rainfall distribution. Such information could facilitate decision-makers to effectively devise plan and establish strategies towards the development of hydrological systems. In this study, time series analysis technique, the double exponential smoothing is applied to rainfall time series at three stations in the state of Sabah, Malaysia. Rainfall data (2000 –2014) from stations Beaufort, Inanam and Semporna at daily scale are collected and aggregated to bi-weekly scale. Results show that double exponential smoothing model fairly able to capture the pattern of rainfall at the selected stations. Forecast results show that for the next twenty four periods, rainfall seems to increase.*

Keywords: Sabah**,** Time Series, Double Exponential Smoothing, Bi-weekly Scale

1.0 INTRODUCTION

Rainfall is the meteorological phenomenon which greatly affects human activities. It is also the main environment element which influences the development of economic activities of a region [1]. Studies of rainfall such as analysis and data simulation are important and could be used as input in making decision towards the planning, design and operation of the hydrologic systems. This includes the constructions of hydrological structures such as damn and bridges [2].

Various approaches on modelling of rainfall series have been conducted in Malaysia using stochastic models and deterministic models. Published works include those focusing on profiling, modelling and generating rainfall series [3-5] at different time scales. However, most of these studies are done in Peninsular Malaysia while not much works have been conducted in Eastern Malaysia. One of the approaches in analyzing rainfall is the time series method. Apart from generating rainfall data, time series modeling facilitate in the planning and managing of water resources, exploring climatic variations, forecasting and estimating missing data. There are some studies using time series analysis in Malaysia, such as studies on rainfall volatility using Seasonal Autoregressive Moving Average model [6], and investigating trends using Holt–Winters method [7].

In this study, time series forecasting model, particularly, Exponential Double Smoothing Method is used to analyze the pattern in the state of Sabah, Malaysia. This study is a valuable contribution since there are insufficient research works on Sabah rainfall series. Most of the research works on rainfall are concentrating in Peninsular Malaysia which has different rainfall profile.

2.0 METHODOLOGY

2.1 Study Area and Data Collection

The land of Sabah which part of the Borneo Island, is located in a tropical geography with equatorial climate. It experiences two monsoon seasons of northeast and southwest. The northeast monsoon occurs from November to March with heavy rains, while the southwest monsoon prevails from May to September with less rainfall. In addition, it also received two inter-monsoon seasons from April to May and September to October, with a considerable amount of rain from 1,800 millimetres to 4,000 millimetres. Due the size of the state, rainfall characteristics has significant temporal and spatial variation between places. Rainfall data from the year 2000 to the year 2014 for 3 selected rainfall stations is obtained from Department of Irrigation and Drainage (DID) Malaysia. Those stations are Beaufort JPS Station, Inanam Meteorology Station and Semporna Airport Station. These stations are chosen based on the completeness of data. Rainfall data at daily scale from each station is collected and aggregated to bi-weekly scale. A total of 360 data sets are obtained during the period of 2000 –2014 and are used for the analysis.

2.2 Exponential Smoothing

Exponential smoothing schemes weight past observations using exponentially decreasing weights. One of the variations is the Double Exponential Smoothing

2.2.1 Double Exponential Smoothing

Double exponential smoothing uses two constants and is better at handling trends. Two equations associated with Double Exponential Smoothing.

$$S_t = \alpha y_t + (1-\alpha)(S_{t-1} + b_{t-1}) \quad 0 \le \alpha \le 1 \qquad (1)$$
$$b_t = \gamma(S_t - S_{t-1}) + (1-\gamma)\, b_{t-1} \quad 0 \le \gamma \le 1 \qquad (2)$$

Note that the current value of the series is used to calculate its smoothed value replacement in double exponential smoothing.
There are a variety of schemes to set initial values for$S_t$and $b_t$in double smoothing. $S_1$is in general set to y_1. Here are three suggestions for b_1:

$$b_1 = y_2 - y_1$$
$$b_1 = [(y_2 - y_1) + (y_3 - y_2) + (y_4 - y_3)]/3$$
$$b_1 = (y_n - y_1)/(n-1)$$

3.0 RESULTS AND DISCUSSION

The bi-weekly rainfall at Beaufort, Inanam and Semporna for fifteen years (2000-2014) was subjected to time series analysis. The statistical analysis of the historical data is given in Table 1. From the table, it can be seen that Beaufort and Inanam has a much greater mean compared to Semporna. The maximum values for both places are also much higher. Figures 1(a) -1(c) show the fitted data against the observed data. Based on the graphs, it can be seen that the double exponential smoothing model fairly capture the pattern of rainfall. Information on basic statistics and graphs revealed that all three stations has high variability of rainfall. The model is then used to make 24 bi-weekly forecast of rainfall. The result is as shown in Table 2.

Table 1: Basic statistics for Beaufort, Inanam and Semporna stations at bi-weekly scale

Stations	No. of Observations	Mean (mm)	St. Dev (mm)	Max (mm)
Beaufort	360	155.87	97.10	536.00
Inanam	360	114.20	85.89	527.60
Semporna	360	73.93	83.06	444.50

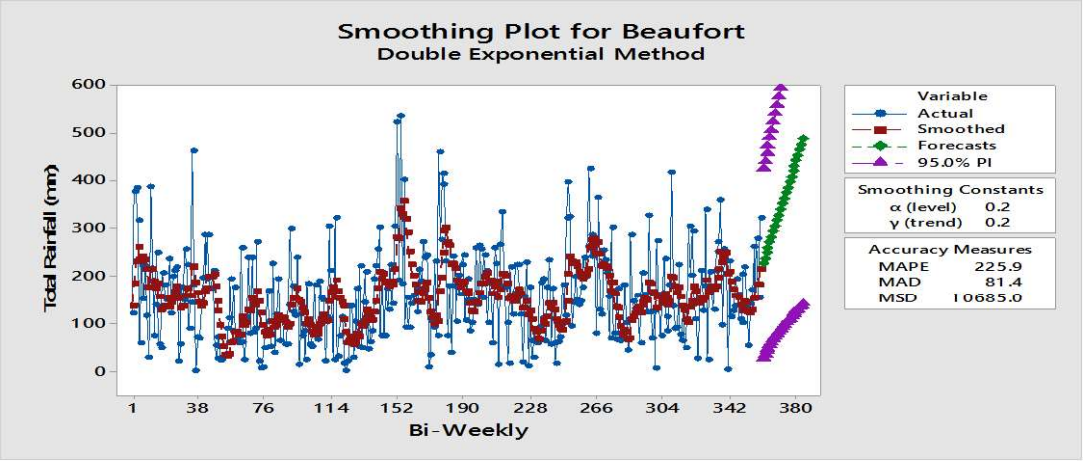

(a) Beaufort

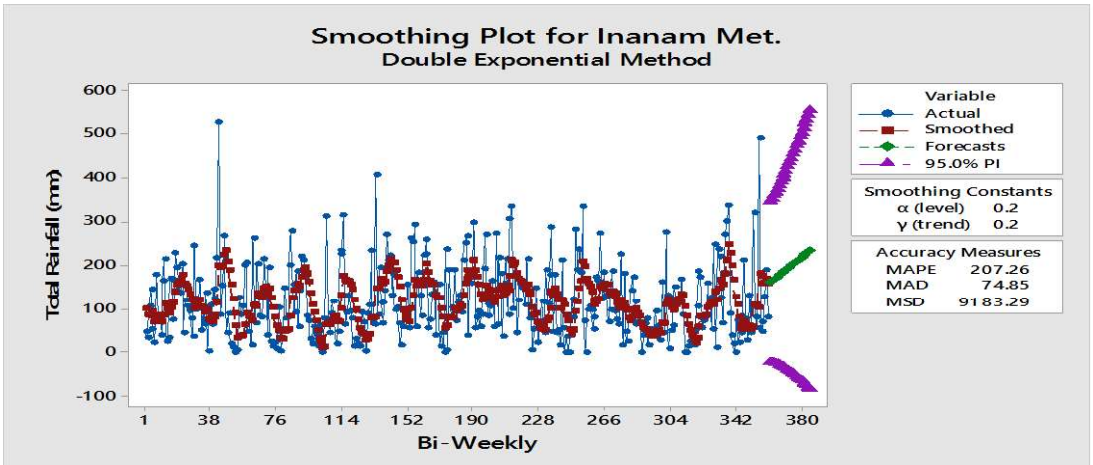

(b) Inanam

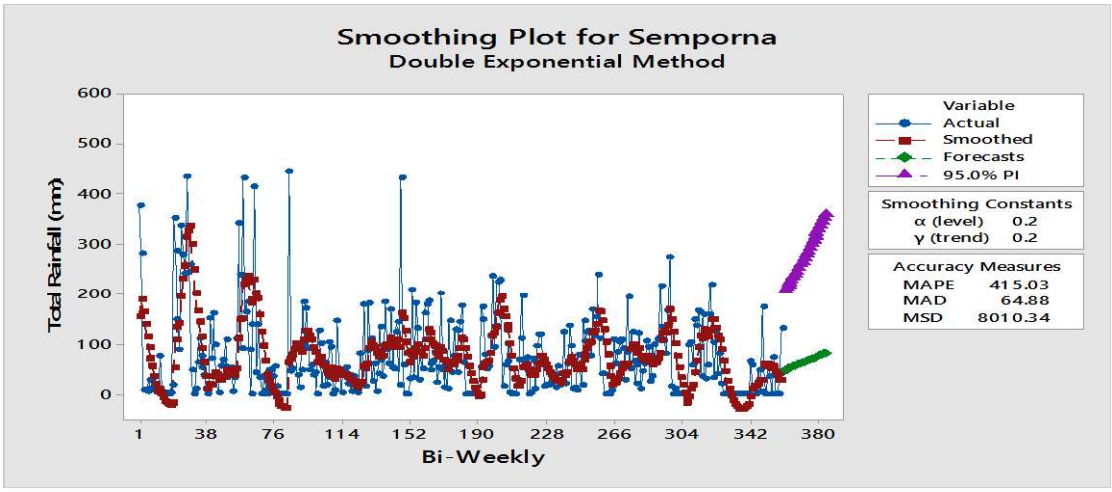

(c) Semporna

Figure 1: Time Series of rainfall at the three stations in Sabah for 2000-2014 period

Table 2: Forecast for 24 bi-weekly periods from 361 to 384 using Double Exponential Method

Period	Beaufort	Inanam	Semporna
361	284.236	96.304	76.79
362	308.243	79.077	95.139
363	332.251	61.851	113.488
364	356.258	44.624	131.837
365	380.266	27.397	150.186
366	404.273	10.171	168.535
367	428.28	7.056	186.884
368	452.288	24.283	205.233
369	476.295	41.509	223.582
370	500.303	58.736	241.931
371	524.31	75.963	260.28
372	548.317	93.19	278.629
373	572.325	110.416	296.978
374	596.332	127.643	315.327
375	620.34	144.87	333.675
376	644.347	162.096	352.024
377	668.354	179.323	370.373
378	692.362	196.55	388.722
379	716.369	213.776	407.071
380	740.377	231.003	425.42
381	764.384	248.23	443.769
382	788.392	265.456	462.118
383	812.399	282.683	480.467
384	836.406	299.91	498.816

4.0 CONCLUSION

Time series analysis plays a significant role in modeling and forecasting of rainfall. It provides vital information to decision-makers to effectively devise plan and establish strategies towards the development of hydrological systems. Time series analysis technique, the double exponential smoothing is applied to rainfall time series at three stations in Sabah. The model is found to be adequate for modeling and forecasting at the three stations. Forecast results show that for the next 24 bi-weekly periods, rainfall seems to increase for all three stations.
The model, however, is moderately able to capture the extreme values. All three stations exhibit high variability of data. Hence, further research is necessary to identify a model that is able to fairly capture the essence of rainfall characteristics in Sabah. Generally, this would lead to a more comprehensive solution to the forecasting problem, including addressing the problem of uncertainty in predictions.

5.0 ACKNOWLEDGMENT

The authors are grateful to the Department of Irrigation and Drainage (DID) Malaysia for providing the precipitation data. This study is funded by GUP Vote 15H74.

REFERENCES

[1] Kripkorir, E.C. “Analysis of Rainfall Climate on the Njemps Flats, Baringo District, Kenya.” Journal Arid Environment 50:445-458. 2004.
[2] Nyatuame, M., Owusu, G., Ampiaw, F. “Statistical Analysis of Rainfall Trend for Volta Region in Ghana”. International Journal of Atmosphere. 2014.
[3] Abas Norzaida, Mohd Daud Zalina & Yusof Fadhilah. “Application of Fourier Series in Managing the Seasonality of Convective and Monsoon Rainfall”. Hydrological Sciences Journal, 61:10, 1967-1980, 2016, DOI: 10.1080/02626667.2015.1062892
[4] Fadhilah Yusof, Norzaida Abas and Zalina Mohd Daud. “Fourier Series in a Neyman Scott Rectangular Pulse Model”. Matematika, 24(2), 237-251, 2008.
[5] Zalina M.D., Nurul Huda M.A., Fadhilah Y., Maizah Hura A., Robiah A and W.Azli WH., 2007. “Exploring the anomalies of rainfall events in the Klang Valley”. National Conference World Water Day 2007, Terengganu, Malaysia, 2007.
[6] Fadhilah Yusof and Ibrahim Lawal Kane, “Modeling Monthly Rainfall Time Series Using ETS and SARIMA Models”. International Journal of Current Research 4(1), 195-200, 2012
[7] Puah, Y.J., Huang, Y.F., Chua, K.C. et al. “River catchment rainfall series analysis using additive Holt–Winters method”, Journal Earth System Science, 125: 269. doi:10.1007/s12040-016-0661-6, 2016.

Modelling of Paddy Production in Malaysia

Kamariah Aliman[a], Norzaida Abas[b] and Wan Normeza Wan Zakaria[c]

UTM Razak School of Engineering and Advanced Technology, Universiti Teknologi Malaysia, Jalan Sultan Yahya Petra, 54100 Kuala Lumpur, Malaysia

[a]Kemm2009@live.com, [b]zaida.kl@utm.my, [c]normeza.kl@utm.my

Abstract - *In Malaysia, paddy production has important role in meeting the nation's food security and socio economic concerns. Since rice is the leading candidate on the list of our food security list, update estimations or forecasting of paddy production is particularly important. The present study aims to identify suitable time series forecasting methods for paddy production. Thirty five years (1980-2014) of paddy data in the form of yearly production are used. Time series forecast methods specifically, single and double exponential smoothing methods and ARIMA model are applied separately to the yearly paddy data and the results are compared. Results show that ARIMA (2,1,2) method is identified as the most appropriate to represent paddy production. Forecast results using the identified model showed that paddy production would experience a small increment trend.*

Keywords: Forecasting, Time Series, Paddy

1.0 INTRODUCTION

The production of paddy plays an important part in the Malaysia's agriculture sector with 85.5% of Malaysia's total paddy production is from the Peninsular Malaysia [1]. Paddy is produced mainly by small holders with an average farm size of about 1.06 hectares [2]. Sixty five percent of the paddy farmers have farms of less than one hectare while only four percent have more than three hectares (Malaysian National Committee of ICID (MANCID)). Paddy is an important crop because rice is the main staple food, accounting about 86% of Malaysia's food grain production. Although the production of paddy has significantly increased from 1,883,604 in 1982 to 2,848,852 in 2014 (Figure 1), the overall production still could not meet the country's demand. Malaysia has to import rice from some other countries such as Thailand and Vietnam. According to the Department of Statistics Malaysia, for 2014 the per-capita consumption of rice was 78.6 kg per year [3]. The self -sufficiency ratio for rice was 71.6% for 2014 compared 71.7% in 2013.

Generally, agriculture information is valuable for Malaysia, however, there were not many studies available on forecasting of crop production. Crop production forecast could contribute to the advancement and improvement of agriculture in terms of farm infrastructure, irrigation facilities and drainage requirements. Since rice is the leading candidate on the list of our food security list, update estimations or forecasting of paddy production is particularly significant. It is the objective of this study to identify

suitable time series forecasting method for the production of paddy. Once the model is identified, it is used to make forecasting on paddy production.

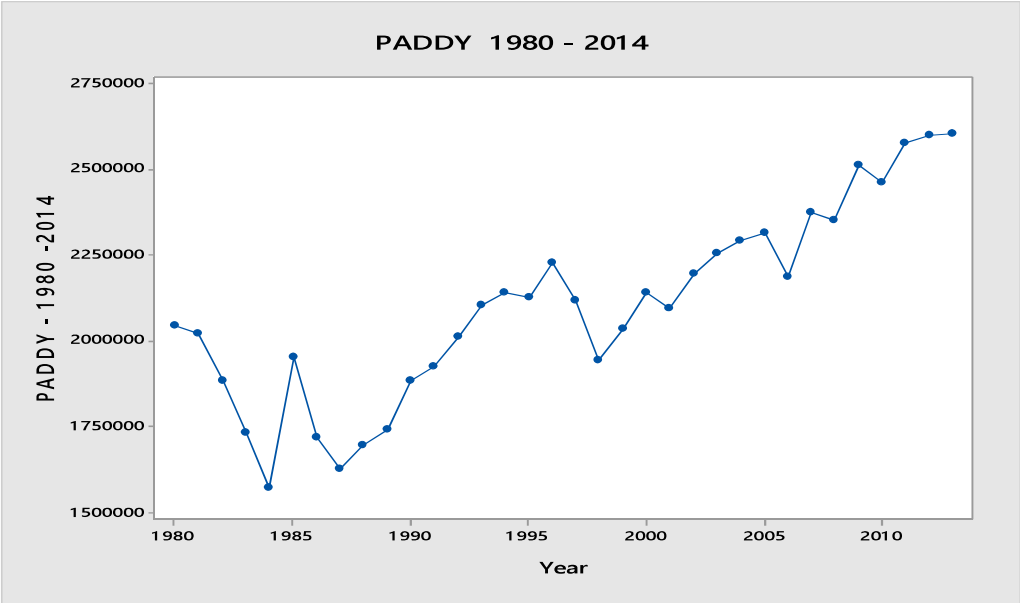

Figure 1: Trend of Paddy production (in metric tonne) for 1980-2014

2.0 DATA AND METHODOLOGY

Thirty five years (1980-2014) of paddy data in the form of yearly production was extracted from the Department of Statistics Malaysia official portal [3]. The trend analysis of paddy production is given in Figure 1.

Time series forecasting method essentially predict future values based on historical data [4,5]. Basically, there are three models used in this study , which are ,single exponential smoothing, double exponential smoothing and ARIMA models. The best model to represent paddy production is chosen based on two assessment criteria namely, Mean Absolute Percentage Error (MAPE) and Mean Absolute Deviation (MAD). The most appropriate model would be the one which has the lowest score in MAPE and MAD tests.

2.1 Trend analysis

Trend analysis is a special case of regression model in which the independent variable is just the time index variable. This method is to fit trend when there is no seasonal component in the series. Ordinary Least Squares Method (OLS) is used to estimate coefficients and the measures of fit of the linear trend model

Model for linear trend is $\hat{y}_t = \beta_0 + \beta_1 t + \varepsilon_t$ (1)
Model for quadratic trend is $\hat{y}_t = \beta_0 + \beta_1 t + \beta_2 t^2 + \varepsilon_t$ (2)

Where $\hat{y}_t$ is the forecast at present time t and ε_t is the error term.

2.2 Exponential Moving Average (Exponential Smoothing)

Exponential smoothing is a forecasting method that weights each value of time series values unequally, with more recent observation being weighted more heavily than more remote observations or weights past observations with exponentially decreasing weights to forecast future values.

2.2.1 Single Exponential Smoothing

Single exponential smoothing is the smoothed version of moving average.

$$\hat{y}_{t+1} = \alpha y_t + (1-\alpha)\hat{y}_t \quad (3)$$

Where ; $\hat{y}_{t+1}$ = the forecast for the next time period
$(t+1)$ $\hat{\hat{y}}_t$ = the forecast for the present time period (t)
y_t = the actual value for the present time period
α = exponential smoothing constant

2.2.2 Double Exponential Smoothing

Double exponential smoothing is used to forecast a time series described by a linear trend and irregular fluctuation (but having no seasonal variations).

$$\hat{y}_t = L_{t-1} + T_{t-1} \quad t = 2,3,4,.. \quad (4)$$

Where $L_t = \alpha y_t + (1-\alpha)\hat{y}_t$ and $T_t = \beta(L_t - L_{t-1}) + (1-\beta)(T_{t-1})$ and
L_t = The smoothed level for time period
T_t = The smoothed trend estimates for this time period
$\hat{y}_t$ = The forecast value at time t
α and β = level and trend smoothing constant

2.3 Auto Regressive Integrated Moving Average (ARIMA)

Auto regression (AR) is a multiple regression technique in which the independent variables are time lagged version of the time dependent variable

$$\hat{Y} = b_0 + \emptyset_1 Y_{t-1} + \emptyset_2 Y_{t-2} + \cdots + \emptyset_n Y_{t-n} + \delta \quad (5)$$

where δ is the error term of the model and $\emptyset_1, \emptyset_2, \ldots$ are coefficient of AR terms

Moving average (MA) term is the number of terms that describe the persistence of a random shock from one observation to the next. A model with two moving average terms (q= 2) is one in which an observation depends on two preceding random shocks.

$$\hat{Y}_t = \varepsilon_t + \theta_t \varepsilon_{t-1} + \theta_{t-1}\varepsilon_{t-2} + \cdots + \theta_n \varepsilon_{t-n} \quad (6)$$

Where θ is the coefficient of MA terms and ε is the residual or error term

Then , $\hat{y}_n = \delta + \sum_{i=1}^{p} b_i y_{t-i} + \epsilon_t + \sum_{j=1}^{q} \theta_j \varepsilon_{t-j}$ (7)

When the time series data is not stationary, data are differenced in order to transform them to become stationary. This results in an "integrated" ARMA (i.e. ARIMA) model, denoted by ARIMA(*p*, *d*, *q*) , where *d* is the order of differencing. There are three major steps to build ARIMA model, which are model identification, parameter estimation, and diagnostic checking [4]. In model identification, the possible model could be moving average, autoregressive model or mix of this model. Autocorrelation function (ACF) and partial autocorrelation (PACF) can be applied to make the first guess. Once the model is identified, the parameter needs to be estimated, and in principle the parameter must be significant and generate lowest residual. A common method is to test the randomness of the residuals using Ljung–Box Statistics, and non-significant p-values indicate that the residuals are uncorrelated and the proposed model is suitable for fitting the historical data.

3.0 RESULT AND DISCUSSION

The trend of paddy as given in Figure 1 revealed that the production of paddy has gradually increased over time. Figures 2a and 2b show the estimated value against observed value using Single Exponential Smoothing, Double Exponential Smoothing models. ARIMA model is also fitted into the data. Results from Augmented Fuller Dickey Test revealed that paddy production data is not stationary, hence the first or second differencing is needed to transform to stationary time series. It was found that differencing of 2 is needed, and ARIMA(2,1,2) is the appropriate ARIMA model. Figure 3 shows the comparison of estimated and observed data using ARIMA (2,1,2) model.

Numerical comparison using MAPE and MAD (Table 1) revealed the scores are not very much different, however ARIMA (2,1,2) model has the lowest score for both tests. The forecasting values are then generated based on ARIMA (2,1,2) model (Table 2).

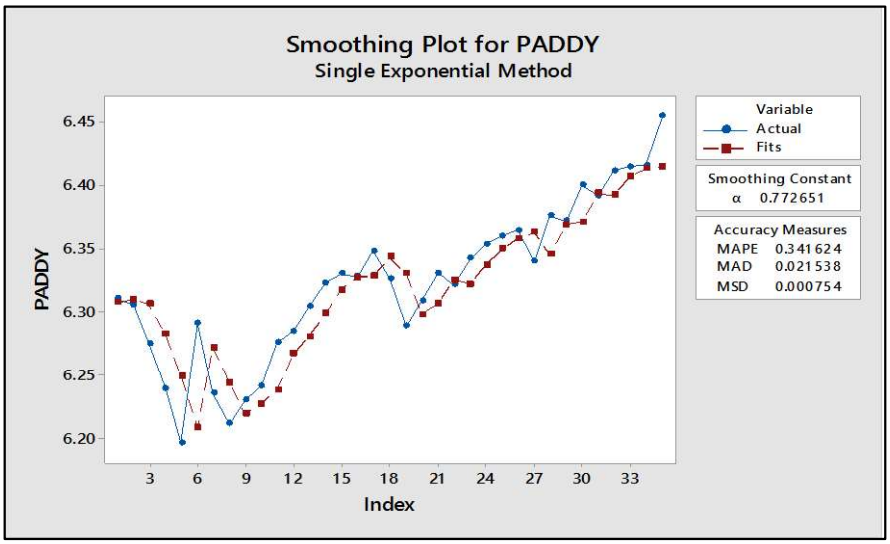

(a) Single Exponential Method

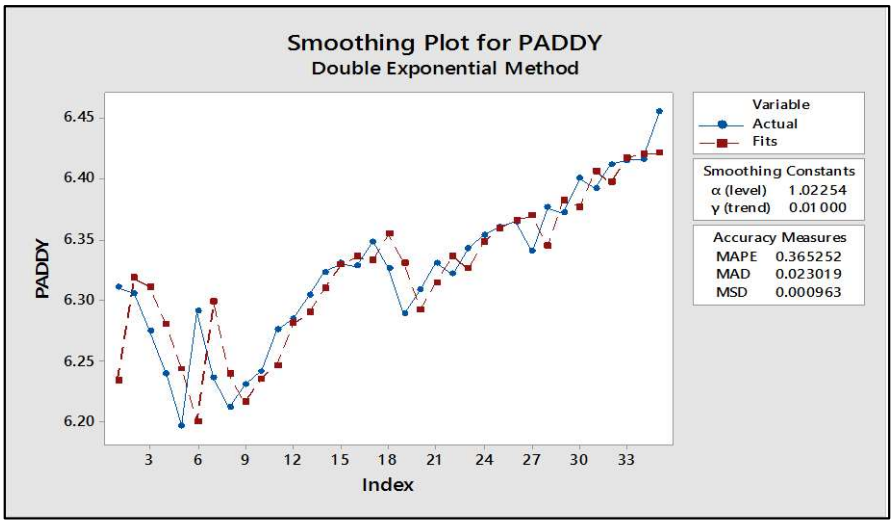

(b) Double Exponential Method

Figure 2 : Graph of Single Exponential Method and Double Exponential Method

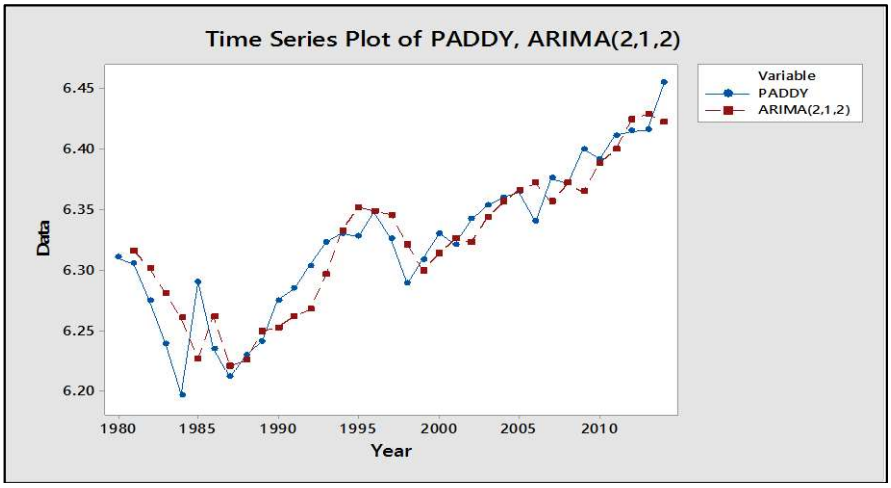

Figure 3: Graph of ARIMA(2,1,2)

Table 1: Comparison of Time Series models

Type Of Crops	Type Of Model	MAPE	MAD
Paddy	Single Exponential Smoothing	0.3410	0.0214
	Double Exponential Smoothing	0.3650	0.0230
	ARIMA (2,1,2)	**0.3090**	**0.0195**

Table 2: Forecast for paddy production

Year	Production (tonne)
2015	2,741,069
2016	2,708,507
2017	2,789,652
2018	2,897,077
2019	2,935,553
2020	2,908,372

4.0 CONCLUSION

Time series forecasting method is well implemented in this study for forecasting yearly production of paddy in Malaysia. The results revealed that the performance of Single Exponential Smoothing, Double Exponential Smoothing and ARIMA(2,1,2) models are quite similar. Closer inspection using MAPE and MAD, identified the ARIMA(2,1,2) model to be the best model to represent paddy production.

Forecast results using ARIMA (2,1,2) show that overall, there would be an increase in the production. The production of paddy in the future is projected to decrease from 2015 to 2017 but it increases in 2018 and 2019 but decrease again in 2020. The expected paddy production in Malaysia in 2020 is 2,908,372 tonne with the expected population 33.82 million by using econometric model.

The predicted result or forecast value could be used by relevant parties such as policy makers to foresee ahead of time the future requirement of import/export crops in Malaysia and enable them to make better strategic planning. The forecast of production also could be beneficial to help the related agencies in estimating the future price of paddy and cost production.

ACKNOWLEDGEMENT

We would like to thank UTM for supporting this study. This study is funded by the GUP Vote 15H74.

REFERENCES

[1] R. B. Radin Firdaus, Ismail Abdul Latiff and P. Borkotoky, 2012, The Impact of Climate Change Towards Malaysian Paddy Farmers, Journal of Development and Agricultural Economics Vol. 5(2), pp. 57-66,

[2] Man and Sadiya, 2009 , Off-Farm Employment Participation Among Paddy Farmers In The Muda Agricultural Development Authority And Kemasin Semerak Granary Areas Of Malaysia, Asia-Pacific Development Journal, Vol. 16, No. 2, 141-153

[3] Department of Statistics Malaysia, 2016, Siri Masa, http://www.dosm.gov.my/v1/

[4] Bruce L Bowerman and Richard T O'Connell, 1987 , Time series Forecasting, Second Edition, Duxbury Press Boston, page 205 -292
[5] C.Chatfield , 1984 , The analysis of Time Series Forecasting, Third Edition, Chapman and Hall, ISBN 0412 26030 1 , page 84-92

Multivariate Analysis of International Baccalaureate (IB) Results in Kolej MARA Banting (KMB)

Mazlina Abd Razak[a], Zalina Mohd.Daud[b] and Normawati Mohd Shariff[c]

UTM Razak School of Engineering and Advanced Technology,UniversitiTeknologi Malaysia, Jalan Sultan Yahya Petra, 54100 Kuala Lumpur, Malaysia

[a]*mazlinaabdrazak@yahool.com.my,* [b]*zalina.kl@utm.my,* [c]*normawati.kl@utm.my*

Abstrac - *This study addressed the issue of declining academic performance among students enrolled in the International Baccalaureate (IB) Diploma Program at Kolej MARA Banting (KMB). It attempted to validate the existence of the decline and identify factors that affect the students' performance. IB results from 1993 to 2016 were source from KMB database. The Mann Kendall Test confirmed existence of a downward trend in the results. Correlational analyses were conducted on 6 subjects that contributed to the total points of IB examination for two main programs which are Engineering and Medicine programs. It was found that high level subjects comprising of the High Level Chemistry, High Level Physics, High Level Biology and High Level Mathematics are highly correlated to IB examination results. This is accentuated further after a policy change in 2009 of which the Medicine program switched to Standard Level Mathematics but the Engineering program continued with the High Level Mathematics. Finally, future performance for the next three years was forecasted using time series analysis using ARIMA (1,0,0). It is anticipated that the findings of this study will provide the relevant authorities with invaluable information regarding student intake and academic performance.*

Keywords: International Baccalaureate, Academic Performance, Trend.

1.0 INTRODUCTION

Research on student performance has always been in the forefront of academic communities. Studies have shown that there is a general decline of Malaysian students such as in Performance of International Students Achievement (PISA) 2012 where Malaysia was ranked number 52 out of 65 countries in the international assessment programme [1]. Trend in International Mathematics and Science Study, (TIMSS) 2011 International Results in Science reported that, Malaysia along with other five countries namely Hungary, Macedonia, Norway, Sweden and Thailand has decreasing trend from 1995 to 2011[2].

The above mentioned findings are a source of concern for Kolej Mara Banting (KMB) as there is a general suspicion of a declining trend in students' results over the past

years. As one of Malaysia's top provider of pre-tertiary education for students who are selected to pursue further studies overseas, ensuring consistent student performance is one of the college's top priority. Hence, it is imperative that empirical analysis based on actual data of students' achievements at KMB be done to address the issue. Long term trends in academic performance and spending are valuable tools for evaluating past education policies and informing current ones [3]. Therefore, findings of this study will provide related authorities valuable evidence regarding the issue and for them to propose actions on improving the existing system.

2.0 METHODOLOGY

Data was sourced from KMB database involving 5993 students for the past 23 years. For the purpose of this study, only results of Engineering and Medicine students are considered. Data comprises of IB total points, grades from High Level Chemistry, High Level Biology, High Level Physics, High Level Mathematics, Standard Level Malay, Standard Level English, Standard Level Economics, Standard Level Business and Management (BMS), and Information Technology and Global Society (ITGS). KMB started operation in 1992 but only data from 2002 onwards are used in the analysis since things were not fully in place in the earlier years of operation.

Data taken is about IB results in KMB. The maximum IB total points is 45 points which comprises of six subjects groups and three matrix points from three skill based subjects, comprising Theory Of Knowledge (TOK), Creativity, Action and Service (CAS) and Extended Essay (EE). The maximum grade in every subject is grade 7, which in total for the six subjects is 42 points. Another 3 points (matrix points) come from TOK, CAS and EE. 35 points is the cutting points for the students to be sponsored abroad.

2.1 Pattern of the IB results in KMB from 2002 to 2016.

For this study, the graphical analysis was done to detect trend. The Mann-Kendall Test was used to confirm whether there was indeed a declining trend in the IB results of KMB. Trend analysis was used to analyse the results from 2002 to 2016. Wimmer & Dominick, [4] stated that trend studies can be limited due to the use of data from samples at different points in time but the method can be useful for considering patterns of overall stability and change over time across different samples. Rosenberg [5] used trend analysis in epidemiologic research, which also useful for educational policy research to identify existing patterns. Apart from that, it can provide a broad perspective of aggregate demographic and geographic data over a period of several years. A more detailed analysis was done on results of Engineering and Medical programmes individually. The same method was also used to study the pattern of grades obtained for the higher level subjects and the standard level subjects.

2.2 Correlation studies on the subjects involve with the IB total points.

Correlation studies are done between the 6 subjects involved and the IB total points results in KMB. To see more specific, it also done to the subjects involved in the two programs tested in this study, which is engineering and medicine programs.

2.3 Forecasting the future results.

In this part, time series analysis was used to forecast the IB results of KMB for the following three years. In doing this, a suitable model has to be determined in order to get a good prediction. Autocorrelation Function (ACF) and Partial-Autocorrelation Function (PACF) values are used in determine an appropriate ARIMA(p,d,q) model. Based on the chosen model, future results of IB total points in KMB will be forecasted.

3.0 RESULTS AND DISCUSSION

Data sourced from KMB database comprises of results from 5993 candidates who has taken the IB examination in KMB from 1993 until 2016 as shown in Table 1. As mention earlier, the maximum IB total points is 45 points which comprises of six subjects groups and three matrix points from three skill based subjects, comprising TOK, CAS and EE. The maximum grade in every subject is grade 7, which in total for the six subjects is 42 points. Another 3 points (matrix points) come from TOK, CAS and EE. 35 points is the cutting points for the students to be sponsored abroad. From six subjects group taken, each student need to choose 3 high level subjects and 3 standard level subjects.

In IBDP, Standard Level courses exposed students to a range of disciplines that they might otherwise opt out of, and High Level courses will allow students to spend more time with subjects they are more interested in by exploring options in addition to the Standard Level core curriculum. To look further, analysis based on high level subjects and standard level subjects was done to see which group of subject influence the results most.

Table 1: Number of candidates from 1993 to 2016 in KMB

Year	1993	1994	1995	1996	1997	1998	2000	2001	2002	2003	2004	2005
No.of Candidates	72	45	51	116	200	99	85	23	127	284	350	455
Year	2006	2007	2008	2009	2010	2011	2012	2013	2014	2015	2016	Total
No.of Candidates	425	378	358	338	321	406	372	392	404	333	359	5993

IB total points of KMB for the past 23 years displayed in the boxplots in Figure 1 revealed the performance of the students in KMB. For the boxplots from 1993 to 1998, most of the students scored below 35 points. In contrast, the boxplots 2002 onwards show a stable achievement of the KMB IB examination result. The first few years of operation cannot take into the consideration since during that time, things were not in place yet. Lack of facilities and man power led to unstable results from 1993 to 2000. Results of 2001 is also excluded since the number of candidates in that year was too small, only 23 students, which led to an unusually higher achievement as displayed in Figure 1. Therefore, the trend analysis was only done on IB total point results from 2002 to 2016.

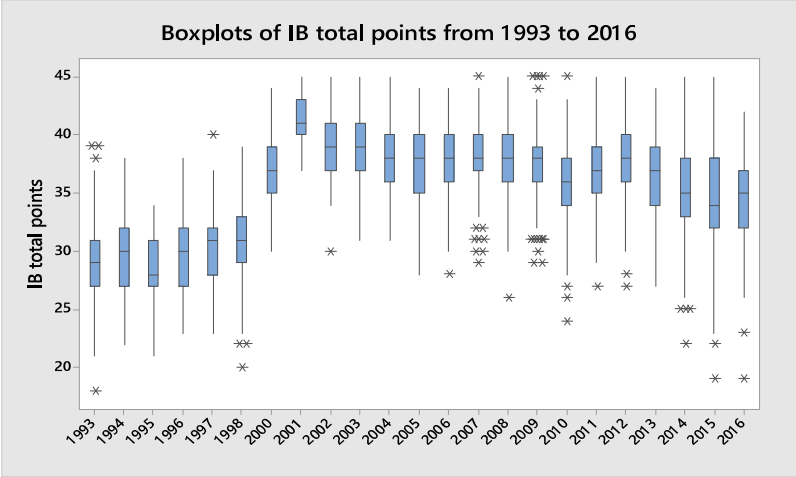

Figure 1: Boxplots of IB total points in KMB 1993-2016.

A plot of the mean total points as shown in Figure 2 shows that there was a declining trend in the results. To confirm this, Mann Kendall Test was done and the results confirm there is a significant trend in the series for the last 15 years, with a p-value <0.05. From Table 2, the Kendall's tau value of –0.752 tells us that there is a downward trend.

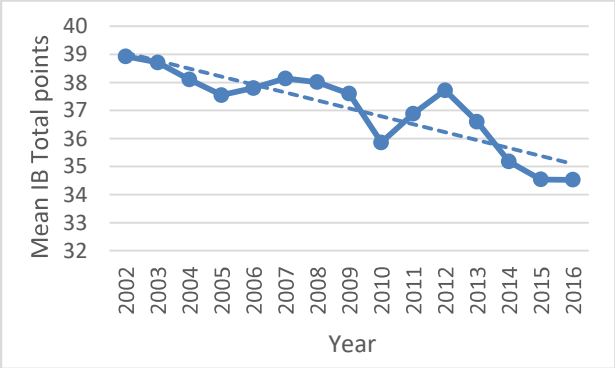

Figure 2: Trend of IB total points in KMB

Table 2: Output for Mann Kendall

Mann-Kendall trend test / Two-tailed test (mean total points):	
Kendall's tau	-0.752
S	-79.000
p-value (Two-tailed)	0.000
alpha	<0.0001
The p-value is computed using an exact method.	

In conjunction with this, as the IB total points decreased, the percentage of students scoring below 35 points increases. It is important to note that students, who scored below 35 points, will fail to secure a scholarship for studies abroad. Looking at Figure 3, the numbers are worrisome. From 2002 onwards, the percentage of students scoring below 35 points do not show any sign of improvement.

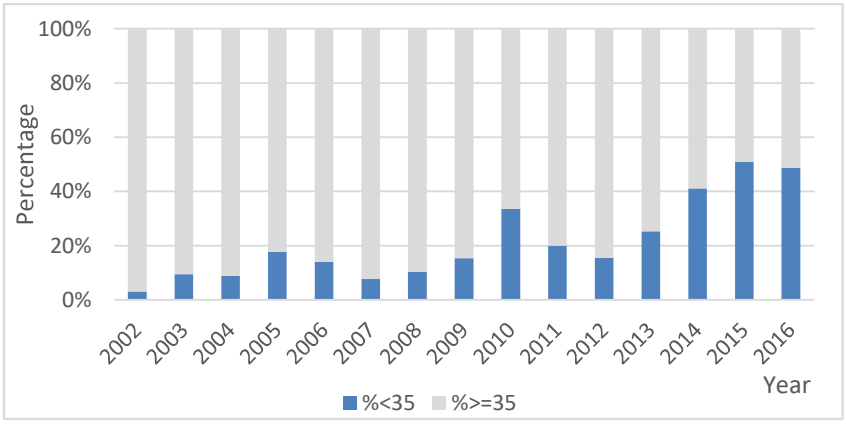

Figure 3: Percentage of KMB students scored below and above 35 points.

The results of high level subjects and standard level subjects are shown in Figure 4 and 5. From the graph, obviously we can see that the high level subject which are known as critical subjects have a declining trend. The graph of high level subjects going towards below grade 5. While standard level subjects are consistently good because they just fluctuate between grade 5 and 7. These suggest that the high level subjects could be a contributing factor on the decreasing IB total points results in KMB.

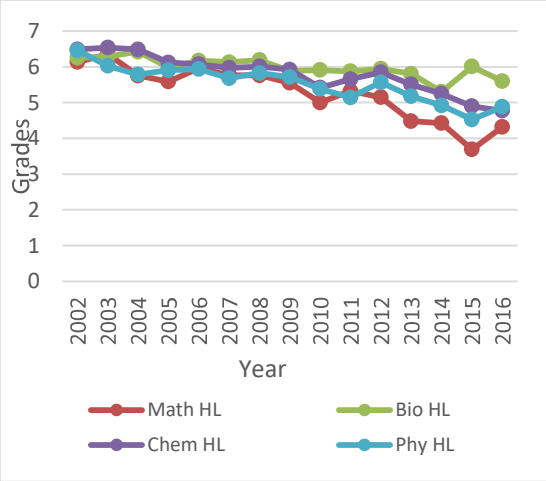

Figure 4: Performances of High Level subjects in KMB 2002-2016

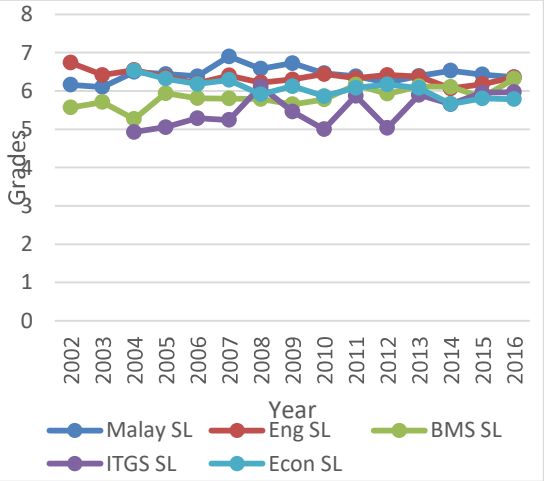

Figure 5: Performances of Standard Level subjects in KMB 2002-2016.

Next is the correlation study on the subjects involved towards the IB total points results. The analysis is done separately between the engineering and medicine programs. The results are shown in Figures 6 and 7.

From the Minitab output for engineering course, the high level subjects are shown to have very high correlation with the IB total points in KMB. The Pearson correlation coefficient exceeds 0.8 for Mathematics high level, Physic high level and Chemistry high level versus the IB total points. While for medicine program, all the high level subjects show there is correlation towards the IB total points, but it is not as high as engineering program results.

The results obtained points to the fact that the higher level subjects are affecting the overall results of KMB, especially for the engineering program. Figure 8 gives a plot of the mean total points of both engineering and medicine courses over the years 2004-2016. By comparing both programs, it is shown that medicine program always perform better than the engineering program throughout the years even though in 2009, there was a policy change in subject combination for medicine program in KMB; the medicine program switch to standard level Mathematics, while the engineering students continued with the high level Mathematics. This finding tells us that the engineering students were having some difficulties in their achievement.

Correlation: TotPtsIB, MATH HL, PHY HL, CHEM HL, MALAY SL, ENG SL, SUB 3

	TotPtsIB	MATH HL	PHY HL	CHEM HL	MALAY SL	ENG SL
MATH HL	**0.862**					
	0.000					
PHY HL	**0.864**	0.798				
	0.000	0.000				
CHEM HL	**0.867**	0.775	0.783			
	0.000	0.000	0.000			
MALAY SL	0.328	0.198	0.151	0.175		
	0.000	0.000	0.000	0.000		
ENG SL	0.456	0.248	0.298	0.261	0.074	
	0.000	0.000	0.000	0.000	0.013	
SUB 3	0.581	0.348	0.380	0.410	0.139	0.284
	0.000	0.000	0.000	0.000	0.000	0.000

Cell Contents: Pearson correlation
P-Value

Figure 6: Minitab output on Correlation between subjects and total points forEngineering program

Correlation: Tot Pnts, Math HL, Bio HL, Chem HL, Malay SL, Eng B SL, Subject 3

	Tot Pnts	Math HL	Bio HL	Chem HL	Malay SL	Eng B SL
Math HL	**0.667**					
	0.000					
Bio HL	**0.711**	0.407				
	0.000	0.000				
Chem HL	**0.764**	0.516	0.616			
	0.000	0.000	0.000			
Malay SL	0.280	-0.005	0.087	0.082		
	0.000	0.766	0.000	0.000		
Eng B SL	0.468	0.079	0.332	0.303	0.090	
	0.000	0.000	0.000	0.000	0.000	
Subject 3	0.560	0.318	0.254	0.263	0.068	0.126
	0.000	0.000	0.000	0.000	0.000	0.000

Cell Contents: Pearson correlation
P-Value

Figure 7: Minitab output on Correlation between subjects and total points for medicine program.

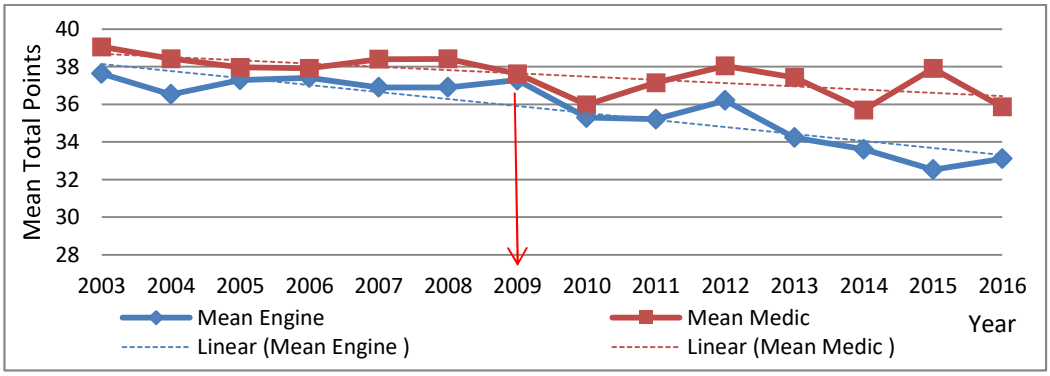

Figure 8: Mean total points of engineering and medicine students in KMB

The last part of this study is to forecast on the future IB total points results in KMB. Using time series analysis, through the ACF graph, it is an exponential decay, which give the idea that we might use the ARIMA model since the ACF with large spikes at initial lags that decay to zero and PACF with large spikes at the first indicates an autoregressive process**.** Next, partial autocorrelation function used to identify the components for an ARIMA model.

From the Partial-Autocorrelation, only the first lag is significant, and then it dropped to zero. By looking at both graphs ACF and PACF in Figure 9 and Figure 10, clearly we can identify a clear lag 1 autocorrelation. The data is a stationary time series, since the ACF is drop to zero relatively quickly.The above ACF is "decaying", or decreasing, quickly, and remains well below the significance range (red lines). This is indicative of a stationary series. This give the idea that the best model to use to do the forecast is ARIMA(1,0,0). Using ARIMA(1,0,0), the results is in Figure 11.

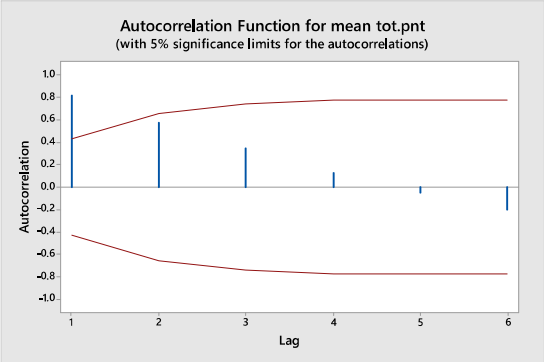

Figure 9: ACF of KMB IB total points

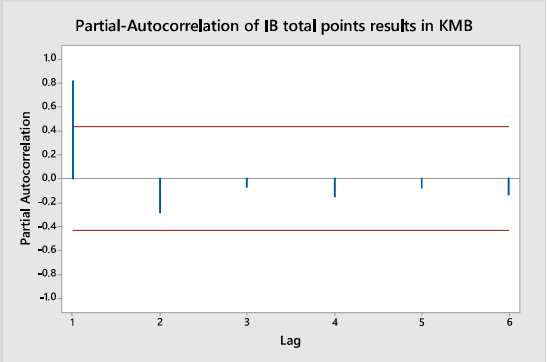

Figure 10: PACF of KMB IB total points

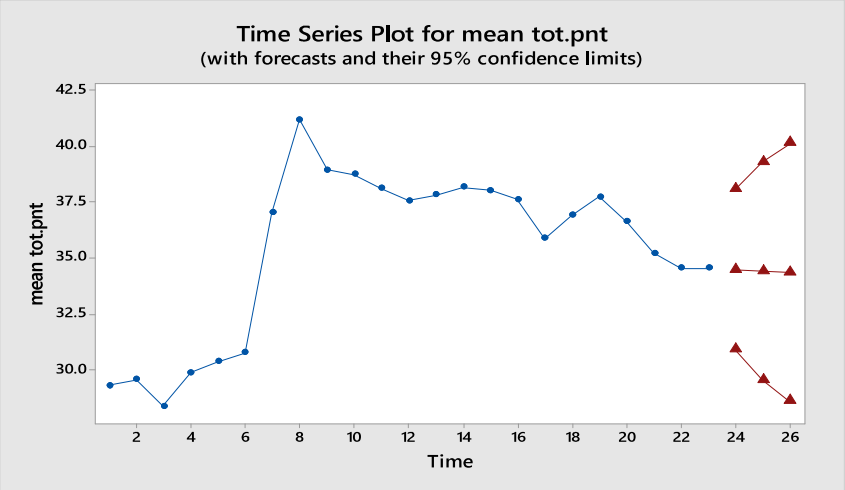

Figure 11: Time series graph of IB average total points in KMB using ARIMA(1,0,0)

The forecasted for the next three years shows that IB total points have a declining trend. From the analysis, the mean IB total points forecasted for the next three years will be 34.4578 for 2016, followed by 34.3912 in 2017 and 34.3299 in 2018. The 95% confidence limits denote it can go as low as 30.8655 and as high as 38.0501 for 2017. Of course these are forecast under the current scenario that is everything is as status quo. If other factors involved such as introduction of new revision program or any changes made on the curriculum, the results will be different.

4.0 CONCLUSION

It was confirmed that IB performance in KMB is having a declining trend. This pattern of results was seen almost every year throughout the study period. It was also observed that the Chemistry HL, Physics HL, Biology HL and Mathematics HL are following the same trend too. The declining of the mathematics and sciences subjects in KMB is significant with the results of PISA 2012 and TIMSS 2011. In relation with this, sponsors or related authorities might need to put in place a more stringent procedure for the process of students' intake so that those selected is really worthy and able to succeed in this program.

Over the study period, high level subjects seem to have problem for the current situation, especially Mathematics High Level. From the correlation studies done, high level subjects are highly correlated towards the IB total points results. Comparing the two programs, students from the engineering program having higher correlation towards the IB total points results. This is related to the performance of engineering students that are always lower than medicine students. KMB management and teachers need to find out the reasons for the engineering students' having difficulties leading to the poor performance, so that appropriate action can be taken to eliminate the problem. On top of that students who are taking high level subjects might need to put in more effort to enhance their understanding of the subjects. Individual commitment is most necessary at this juncture.

The forecasted result suggests that there will unfortunately be further deterioration of KMBs' results. Hence it is time for the related authorities such as the Parents Teacher Association, Education Ministry and all educational stakeholders involved working together and finding solutions for the betterment of KMB.

REFERENCES

[1] Angel Guria (2014),"PISA 2012 Results in Focus: What 15-year-old know and what they can do with what they know".

[2] Michael O.Martin, Ina V.S Mullis, Pierre Foy and Gabrielle M.Stanco. (2011), "TIMSS International Results in Science:Trend in International Mathematics and Science Study".

[3] Andrew J. Coulson. March (2014), "State Education Trend: Academic Performance and Spending over the past 40 years". Policy Analysis CATO Institute No 746.

[4] Wimmer, R.D. & Dominick., J.R. (2011). Mass media research: An introduction. Boston: Wadsworth

[5] Rosenberg, D. (1997). Trend analysis and interpretation.Division of Science, Education and Analysis, Maternal and Child Health Bureau, Department of Health and Human Services.
http://mchb.hrsa.gov/publications/pdfs/trendanaylsis.pdf

Analysis of Dengue Cases in Johor State, Malaysia

Rafidah Muhammad Shamsuddin[a], Norzaida Abas[b] and Sharipah Alwiah Syed Abd. Rahman[c]

UTM Razak School of Engineering and Advanced Technology, Universiti Teknologi Malaysia, 54100 Jalan Sultan Yahya Petra, Kuala Lumpur, Malaysia

[a]*rafidah@mrsmag.edu.my,* [b]*zaida.kl@utm.my,* [c]*shalwiah.kl@utm.my*

Abstract – *Dengue fever is a leading public health problem in Malaysia and places a substantial burden in Malaysia. The reported number of dengue cases seemed to be rising each year. In order to minimize dengue fever outbreak, related parties have to plan and prepare resources based on available information and predictions of expected cases. Hence, the present study statistically analyse dengue cases at the state of Johor, Malaysia. Time series models are fitted to dengue data from Johor in order to identify the mathematical model that best describe the data. Subsequently, such model is used to make forecasting on the number of expected cases. For this purpose, Double Exponential and Winters' Method Smoothing were employed to forecast expected dengue cases. Results show that dengue cases are expected to decrease.*

Keywords: Dengue, Time Series, Exponential Smoothing Models, Forecasting

1.0 INTRODUCTION

Dengue fever (DF) is a leading public health problem and imposes a heavy burden in Malaysia. Dengue is a viral infection spread by the aedes mosquitoes with high morbidity and mortality. The symptoms of DF include a high temperature fever, acute headache, feeling nausea, vomiting, widespread of red rashes and pain in the eyes, joints and muscles [1]. While there is no specific treatment for dengue, with relevant medical care, infected patients could be saved [2].

There are many cases detected in tropical and subtropical regions around the world, predominantly in metropolitan areas. The global increase of dengue incidence is also experienced by Malaysia. The outbreaks in Malaysia are at an alarming rate with most cases reported within the cities. The reported number of dengue cases rose each year, from 108,698 cases in 2014 to 120,836 cases in 2015, an increase of 11.2% or 12,138 cases [3]. Most of the reported dengue cases were from urban areas (70% – 80%) where factors such as high density population and rapid development tend to facilitate the transmissions of dengue [3]. Dengue incidence which is a public health issue with high morbidity and mortality rate inadvertently tends to escalate the economic burden. DF has no effective vaccine and only the symptoms of DF can be treated, but not the disease itself. Therefore effective monitoring and forecasting of DF outbreaks is necessary in preventing the spread of DF.

The present study aim to statistically analyse dengue cases in the state of Johor, Malaysia. Time series models are fitted to dengue data in order to identify mathematical model that best describe the data. Subsequently, such model is used to make forecasting on the number of expected cases. In Malaysia, studies using time series analysis and forecasting are still scarce, although some work were done in Kuala Lumpur, Putrajaya and some areas in Selangor using 3 years and less of data [4,5].

2.0 DATA AND METHODOLOGY

2.1 Data

Johor is located at the southern part of Peninsular Malaysia. It is considered one of the most developed states in Malaysia and in terms of population; it is the second most populous state. Dengue data of about seven years (2010 – 2016) is obtained from the official Malaysia i-Dengue Data Portal, provided by the Ministry of Health Malaysia. The duration of data in this study is much longer than similar studies done in Malaysia [6]. Specifically, weekly data from week 8, 2010 to week 46, 2016 (351 weeks) for Johor are used. However there are some missing data, which were infilled using Minitab. The completed data set was then analysed by using double exponential smoothing and Winters' method smoothing, in order to model data pattern and make forecasting on future pattern of dengue cases.

2.2 Exponential Smoothing

Exponential smoothing [7] is a simple but provide a practical approach to forecasting, whereby the forecast is constructed from an exponentially weighted average of past observations. The largest weight is given to the present observation, less weight to the immediately preceding observation, even less weight to the observation before that, and so on.

2.2.1 Double exponential smoothing

Double exponential smoothing technique smooths out the data when a trend is present. Exponential smoothing with a pattern works much like simple smoothing apart from that two components must be updated every period - level and trend. The level is a smoothed estimate of the value of the data at the end of every period. The trend is a smoothed gauge of the estimation of average growth at the end of every period. The specific formula for simple exponential smoothing is:

$$S_t = \alpha * y_t + (1 - \alpha) * (S_{t-1} + b_{t-1}) \; 0 < \alpha < 1 \quad (1)$$
$$b_t = \gamma * (S_t - S_{t-1}) + (1 - \gamma) * b_{t-1} \; 0 < \gamma < 1 \quad (2)$$

Note that the present value of the series is used to calculate its smoothed value replacement in double exponential smoothing. There are numerous techniques to choose the initial values for S_t and b_t. S_1 is in general set to y_1.

Three recommendations for b_1

$$b_1 = y_2 - y_1$$
$$b_1 = [(y_2 - y_1) + (y_3 - y_2) + (y_4 - y_3)]/3$$
$$b_1 = (y_n - y_1)/(n - 1)$$

2.2.2 Holt-Winters Forecasting

Holt's method is used to manage time series when there are trend and seasonal variations. There are two forms in Holt-Winters method, multiplicative and additive, the utilization of which relies on the characteristics of the specific time series [8].

The general forecast function for the multiplicative Holt-Winters method is:

$$\hat{y}_{n+l|n} = (m_n + lb_n)c_{n-s+l} \qquad l=1, 2,\ldots \tag{3}$$

where m_n is the component of level, b_n is the component of the slope, and c_{n-s+l} is the relevant seasonal component, with s signifying the seasonal period (e.g. 12 for monthly data and 4 for quarterly data)

Therefore if a monthly time series is considered, the one step ahead forecast is given by:

$$\hat{y}_{n+l|n} = (m_n + b_n)c_{n-11} \tag{4}$$

The updating formulae for the three components will each require a smoothing constant. If once again α_0 is used as the parameter for the level and α_1 for the slope, and a third constant α_2, is added as the smoothing constant for the seasonal factor, the updating equations will be:

$$m_t = \alpha_0 \frac{y_t}{c_{t-s}} + (1-\alpha_0)(m_{t-1} + b_{t-1}) \tag{5}$$

$$b_t = \alpha_1(m_t - m_{t-1}) + (1-\alpha_1)b_{t-1} \tag{6}$$

$$c_t = \alpha_2 \frac{y_t}{m_t} + (1-\alpha_2)c_{t-s} \tag{7}$$

Once again, α_0, α_1, and α_2 all lie between zero and one. If the aforementioned additive version of Holt-Winters was used, the seasonal factor is simply added as opposed to multiplied into the one step ahead forecast function, thus:

$$\hat{y}_{n+l|n} = m_n + b_n + c_{n-11} \tag{8}$$

and the level and seasonal updating equations involve differences as opposed to ratios:

$$m_t = \alpha_0(y_t - c_{t-s}) + (1-\alpha_0)(m_{t-1} + b_{t-1}) \tag{9}$$

$$c_t = \alpha_2(y_t - m_t) + (1-\alpha_2)c_{t-s} \tag{10}$$

The slope component, b_t, remains unchanged.
Normally, the smoothing parameters are chosen between the range of 0.02 and 0.2.

3.0 RESULTS AND DISCUSSION

The exponential smoothing techniques, specifically the Double Exponential and Winters' methods are fitted to the dengue data of Johor. The results in the form of graphs are given in Figure 1 and 2.

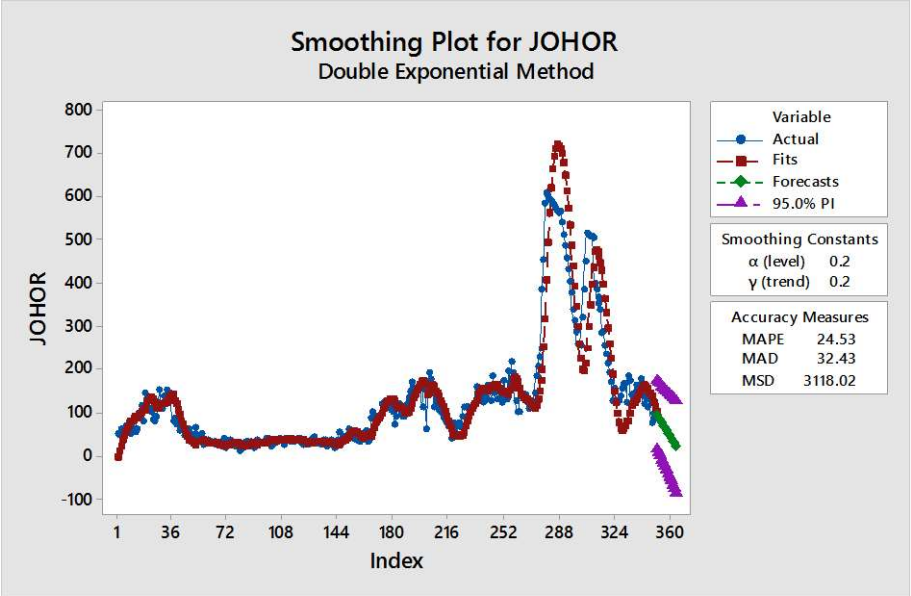

Figure 1: Double Exponential Smoothing Technique

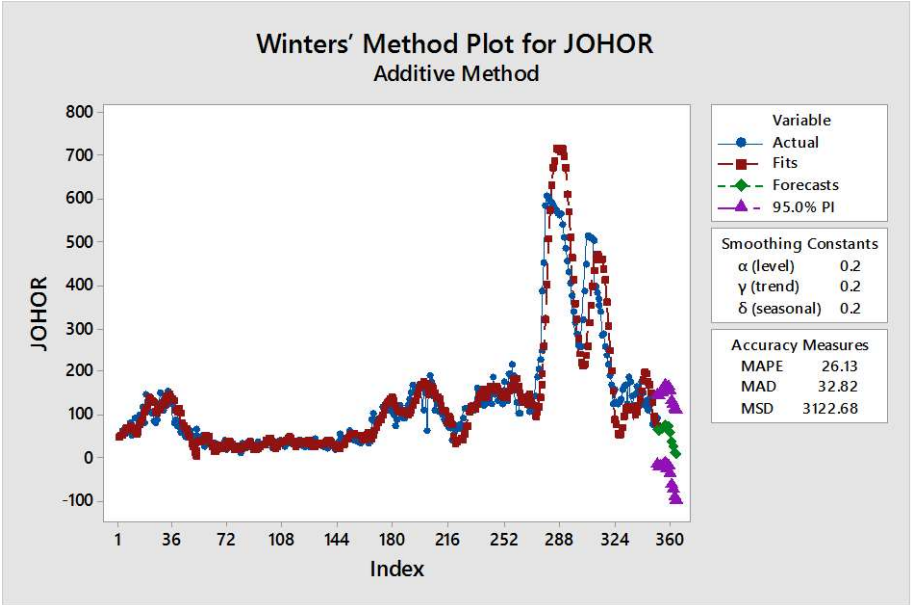

Figure 2: Holt-Winter's Method

From the graphs, it can be seen that the performance of the two methods are almost identical. Numerical comparisons are conducted using three main criteria, namely Mean Absolute Percentage Error (MAPE), Mean Absolute Deviation (MAD) and Mean Squared Deviation (MSD) are shown in Table 1. The lowest value (in bold) indicates the better model. Results show that the values of all three criteria for both models are almost similar, nevertheless the best model is Double Exponential Smoothing. Using Double Exponential Smoothing, forecasting of future dengue cases is conducted for 13 weeks. Results are as shown in Table 2. The forecasted dengue cases for the next 13 weeks are expected to decrease.

Table 1: Comparison of MAPE, MAD and MSD

Accuracy Measures	**Double Exponential Smoothing α (level) 0.2, γ (trend) 0.2**	**Winters' Method (Additive) α (level) 0.2, γ (trend) 0.2 δ (seasonal) 0.2**
MAPE	**24.53**	26.13
MAD	**32.43**	32.82
MSD	**3118.02**	3122.68

Table 2: Forecasting result for week 47, 2016 to week 7, 2017

Week	**Expected Cases**
1	92
2	86
3	80
4	74
5	68
6	62
7	56
8	50
9	44
10	38
11	32
12	26
13	20

4.0 CONCLUSION

This paper presents the comparison of two different exponential smoothing technique that can be used to analyze and forecast the dengue fever cases in Johor. Both models are able to capture the pattern of the dengue cases, however it is identified that Double Exponential Smoothing is the better model. Forecast results of 13 weeks show that expected dengue cases are gradually decreasing.

The outcome of this research could be beneficial to public health officers and relevant authorities to arrange and plan budget to anticipate dengue fever epidemic, subsequently minimize morbidity and mortality. Additionally it is hoped that effective planning could reverse the rising pattern of dengue by upgrading the readiness to recognize, characterize, and contain epidemic rapidly and to stop the transfusion to new zones. Continuous monitoring of dengue status and mortality at all levels is important, as to address uncontrolled circumstance of the disease.

5.0 ACKNOWLEDGMENT

These authors would like to thank the Ministry of Health in providing data of dengue cases in Malaysia.

REFERENCES

[1] Hazrin, Mohd, Helen Guat Hiong, Nadzri Jai, Norzawati Yeop, Muhammad Hatta, Faizah Paiwai, S. Joanita, and W. Othman. "Spatial Distribution of Dengue Incidence: A Case Study in Putrajaya." Journal of Geographic Information System 08, no. 01 (2016): 89-97.

[2] Ministry of Health, Malaysia. "Statement on dengue by Director General of Health", 2014.

[3] Ministry of Health, Malaysia. "Statement on dengue by Director General of Health". 2015.

[4] Husin, Nor Azura, Naomie Salim, and Ab Rahman Ahmad. "Modeling of Dengue Outbreak Prediction in Malaysia: A Comparison of Neural Network and Nonlinear Regression Model." 2008 International Symposium on Information Technology, 2008.

[5] Moore, A., Seng, S.B., Chong, A.K. "Geostatistical Modelling, Analysis and Mapping of Epidemiology of Dengue Fever in Johor State, Malaysia". The 17th Annual Colloquium of the Spatial Information Research Centre, 2005.

[6] Ho, Chiung Ching, and Choo-Yee Ting. "Time Series Analysis and Forecasting of Dengue Using Open Data." Advances in Visual Informatics Lecture Notes in Computer Science (2015): 51-63. Web.

[7] Ostertagová, Eva, and Oskar Ostertag. "Forecasting Using Simple Exponential Smoothing Method." Acta Electrotechnica Et Informatica 12, no. 3, 2012.

[8] Pan, Rong. "Holt-Winters Exponential Smoothing." Wiley Encyclopedia of Operations Research and Management Science, 2011

Effect of Load Carriage on the Lower Limb of Primary School Children

Aida Sabli[a], Sharifah Alwiah Syed Abd. Rahman[b] and Zalina Mohd. Daud[c]

UTM Razak School of Engineering and Advanced Technology , UniversitiTeknologi Malaysia, Jalan Sultan Yahya Petra, 54100 Kuala Lumpur.

[a]aidasabli@yahoo.com, [b]shalwiah.kl@utm.my, [c]zalina.kl@utm.my

Abstract- *School children carried heavy backpack that exceeds their body weight will make them at risk for poor posture and unbalance walking gait. The objectives of this study are to determine the effect of ankle and knee angles and the values of torques at the ankle and knee. A mathematical model of a three-link kinematic chain on the lower limb which consists of thigh, calf and foot is developed using Kane's method and the inverse dynamic method is applied to calculate the values of the torques. Subjects were required to walk on a 6 metre-track with four different load conditions: 0%, 10%, 15% and 20% of their body weight. Results showed that as the load increased, the knee angles keep increasing until produced the highest maximum knee angles in stance phase and lowest decrement in swing phase for load 20% of body weight. Ankle angles showed decrements and produced lowest minimum in stance phase and highest maximum in swing phase in load 20% of body weight. During stance phase the values of torques were at a minimum to compensate with the values at the angles and the lowest torque came from load of 20% of body weight. Values of torque at ankle and knee joint play important role for stability during walking with or without the load carriage.*

Keywords : Kane's Method, Torque, Load Carriage, Primary School Children, Backpack.

1.0 INTRODUCTION

Most studies on human movement about load carriage have been done either on whole body or upper limb. They did their research mostly on adults or in general. Kinoshita [1] examined the effects of distinct loads (multiple-pack and backpack) on selected biomechanical parameters walking gait. The foot rotated anteriorly and posteriorly around the distal end of the metatarsal bones for a lengthy period of time when carrying heavy backpack. Some researchers reported that to take stress off the metatarsal bones, the distance of step should be shortened as the load is increased so that a faster transfer of the body weight from one leg to the other can be achieved. Pascoe et al. [2] studied about load carriage on ten children, 11–13 years of age and found that when they carried a 7.7 kg backpack load (17% of body weight), their stride length significantly decreased and their stride frequency significantly increased compared to a no load condition. Hasyatun et. al. [3] developed mathematical model using Newton Euler on lower limb to produce forces and torques for biomechanics analysis of human movement to avoid injuries in knee and ankle in general.

Biomechanical analysis of the movement under investigation enhances the understanding of human leg morphology and control mechanism in supporting loads and provides a biomechanical framework to identify the muscles and joints that are critically subjected to musculoskeletal injury during load carrying. In addition, muscle energy highlights the design criterion of more efficient, anthropometric and lightweight assistive device structures for load augmentation purposes [4].

Jason et. al. [5] did their studies in lower extremity joint torque during carrying task in children and found that ankle plantar flexion, ankle inversion, knee extension and hip extension torques were significantly increased at 10% and 20% loads of body weight. Sharifah Alwiah et al. [6], developed a model using Kane's method on the upper limb while Rambely and Fazrolrozi [7] did their research on biomechanics model of a six-link kinematic chain of whole human body. In general, many types of mathematical models have been developed to represent human gait movement through Newton Euler method, Kane's method or statistical test on upper limb or whole body but very limited studies were done via Kane's method on lower limb.

Thus, the objective of this paper is to obtain a two dimensional model of lower limb segments which focus on thigh, calf and foot in using Kane's method. By applying inverse dynamic method, values of torques can be determined and analysed at the ankle and knee joint while walking with load carriage.

2.0 METHODOLOGY

Three boys aged 7 to 9 years old with average weight ±29.17 kg and average height ±1.25 m were selected as subjects for this study. The subjects were free from any injuries prior to the experiment consent form. The kinematic data for subject's segment angles which were knee angle and ankle angle were obtained from data of walking movement from the experiment with 0%, 10%, 15% and 20% of body weight. One gait cycle consists of the time from which the heel strikes and touches the ground to the time it touches the ground again. The motion of the subject is divided into two phases; 60% in stance phase and 40% in swing phase.

In this paper, Kane's Method is used in order to determine the two dimensional model of lower limb segments with two degrees of freedom (q1 as ankle angle and q2 as knee angle in degree) in sagittal plane as shown in Figure 1.

Kane's method is a vectorised approach that used vector cross product and dot product to produce velocities and accelerations. A few concepts such as generalised speed, partial velocity, partial angular velocity, generalised active forces and generalised inertia forces had been applied [8].

There are four steps to produce equation in Kane's method. First step, determine the important points which focus on foot as reference frame , calf segment (ankle to knee) and thigh segment (from knee to pelvic). Second step, choose the generalised position, generalised speed and acceleration especially to the important points that already determined. Generalised speed (u_i) = derivative of first order for generalised coordinate of i (q_i) ;

$$u_i = \dot{q}_i \tag{1}$$

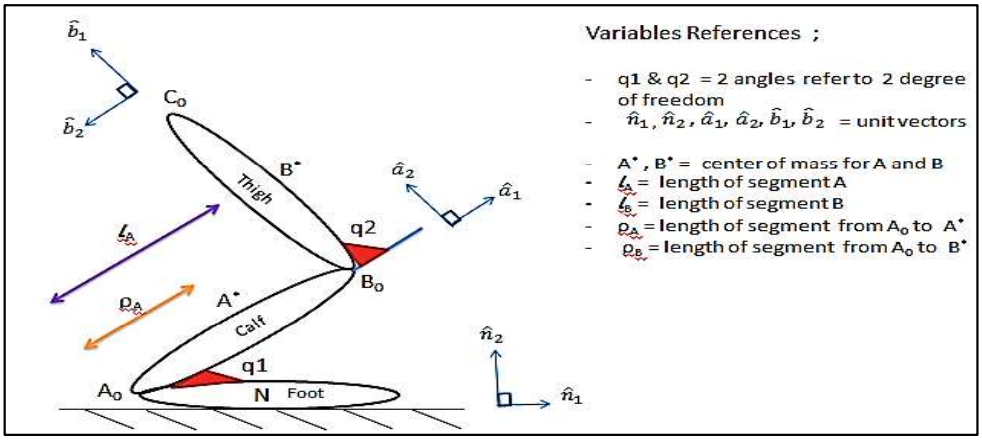

Figure 1: Biomechanical model of 3 segments of lower limb which are thigh, calf and foot (reference frame N)

In third step, form partial velocity equation and fourth step, used generalised speed and partial velocity to obtain generalised active force equation. Dot product operation between partial velocity and active force into the point on the segment and partial angle velocity and torque are applied and added. Generalised active force with degree of freedom, *n* can be shown as below;

$$F_r = \sum_{i=1}^{v}(N_{\vec{v}_r} P_i) \cdot \overrightarrow{R_i}) + \sum_{j=1}^{\mu}(N_{\vec{w}_r} B_j) \cdot (\vec{\tau}_j) \quad (2)$$

where segment $r = 1,2,....,n$

F_r = generalised active force for reference frame *N* system
v = point when force is respond
μ = torque respond on rigid body
$\vec{R}_i$ = summation of all distance and body force (except inertia force)
P_i = no of point $i=1,2,...,v$
$N_{\overrightarrow{v_r}}$ = partial linear velocity to reference frame N
$\vec{\tau}_j$ = torque that respond to each body B_j
B_j = no of body $j=1,2,..,\mu$
$N_{\overrightarrow{\omega_r}}$ = partial angular velocity to reference frame N

and

$$F^*_r = \sum_{i=1}^{v}(N_{\vec{v}_r} P_i) \cdot \overrightarrow{R_i}) + \sum_{j=1}^{\mu}(N_{\vec{w}_r} B_j) \cdot (\vec{\tau}_j) \quad (3)$$

where segment $r = 1,2,....,n$

F^*_r = generalised inertia force for reference frame *N* system
$\overrightarrow{R^*}_i$ = inertia force that respond to each mass centre P^*_i ,
$= -m_{P^*_i} \cdot N_{\vec{\mu}} P^*_i$ where $m_{P^*_i}$ = mass focus on point
$N_{\vec{\mu}} P^*_i$ = acceleration for P^*_i
$\overrightarrow{\tau^*}_j$ = inertia torque that respond to each body $B_j = -I_B N_{\dot{\alpha}} B_j$

$F_r(r = 1,2, \dots n)$ is a generalised active forces that obtained from simplified force, moment and torque and $F^*{}_r(r = 1,2, \dots n)$ is a generalised inertia forces that obtained from simplified force and inertia torque . The total of generalised active forces and generalised inertia forces will produce dynamic equation of motion for *n* degree of freedom system. Generally, for *S* system that have *n* degree of freedom, the existence of *n* number of scalar dynamic equation of motion will represent the acceleration through the system as a function of generalised coordinate and generalised velocity. Motion dynamic equation can be defined as

$$F_r + F^*{}_r = 0 \tag{4}$$

Then dynamic equation of motion for first chain is $F_1 + F^*{}_1 = 0$ and for the second chain, is $F_2 + F^*{}_2 = 0$. Then applying dynamic equation in matrix form;

$$M\ddot{Q} = \vec{T} + \vec{G} + \vec{E} \tag{5}$$

where

M = the mass matrix or inertia matrix that contains mass moment inertia

$\ddot{Q}$ =the acceleration of the nth generalised coordinate $\vec{G}$ = the gravity forces

$\vec{E}$ =external forces exerted on the system $\vec{T}$ = the torque

The valueof torque can be obtained from the dynamic equation by using inverse dynamic equation ;

$$\vec{T} = M\vec{\ddot{Q}} - \left(\vec{G} + \vec{E}\right) \tag{6}$$

where ;

$$M = \begin{bmatrix} m_A{\rho_A}^2 + m_B\left({\rho_B}^2 + {l_A}^2\right) + I_{A^*} + I_{B^*} & m_B{\rho_B}^2 + I_{B^*} \\ m_B{\rho_B}^2 + I_{B^*} & m_B{\rho_B}^2 + I_{B^*} \end{bmatrix} \tag{7}$$

$$\vec{\ddot{Q}} = \begin{bmatrix} \ddot{q}_1 \\ \ddot{q}_2 \end{bmatrix} \tag{8}$$

$$\vec{G} = \begin{bmatrix} m_A g \\ m_B g \end{bmatrix} \begin{bmatrix} -\rho_A \cos(q_1) & -l_A \cos(q_1) - \rho_B(-\sin(q_1)\sin(q_2) + \cos(q_1)\cos(q_2)) \\ 0 & \rho_B(-\sin(q_1)\sin(q_2) + \cos(q_1)\cos(q_2)) \end{bmatrix} \tag{9}$$

$$\vec{E} = \begin{bmatrix} -f_1 l_A \sin(q_1) + f_1 l_B(-\cos(q_1)\sin(q_2) - \sin(q_1)\cos(q_2)) + \\ f_2 l_A \cos(q_1) + f_2 l_B(-\sin(q_1)\sin(q_2) + \cos(q_1)\cos(q_2)) \\ f_1 l_B(-\cos(q_1)\sin(q_2) - \sin(q_1)\cos(q_2)) + \\ f_2 l_B(-\sin(q_1)\sin(q_2) + \cos(q_1)\cos(q_2)) \end{bmatrix} \tag{10}$$

$$\vec{T} = \begin{bmatrix} \left((\hat{a}_3) \cdot \left(\tau_{N/A} - \tau_{A/B}\right)\right) + (\hat{b}_3) \cdot (\tau_{A/B}) \\ (\hat{b}_3) \cdot (\tau_{A/B}) \end{bmatrix} \tag{11}$$

Apart from the calculation above, it was necessary to calculate the physical measurement of the subjects and measurement calculations were referred according to formulae and Anthropometric Data [9].

3.0 RESULTS AND DISCUSSION

Two graphs of knee and ankle angles and two graphs of torque at knee and ankle were showed in Figure 2(a) and Figure 2(b). The positive values of graphs represented flexion direction in angles and torque values of knee and dorsiflexion direction in angles and torque values of ankle.

The negative values represented extension direction in angles and torque values of knee and plantar flexion direction in angles and torque values of ankle.

Analysis description in three phases which involve first 30%, next 30% and after 60% of gait cycle. For first phase, knee angles were flexing until the graphs produced highest maximum angles in 20% load of BW meanwhile plantar flexor of ankle angles produced lowest minimum angles in 15% load of BW. Both graphs of knee and ankle torques decreased at lowest value especially at the ankle that had 20% load of BW before make some increments.

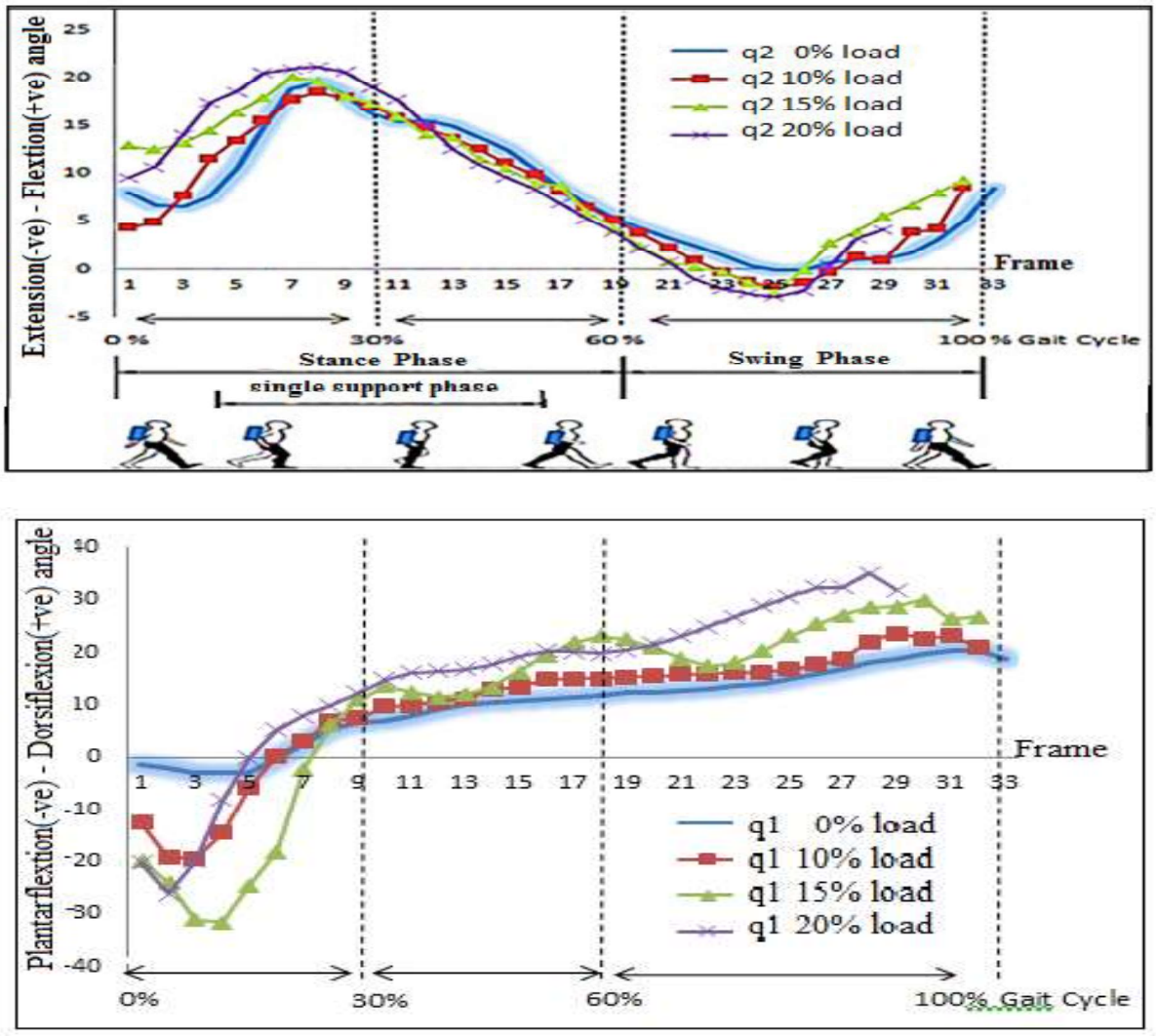

Figure 2(a): Graphs of knee angles (above) and ankle angles (below)

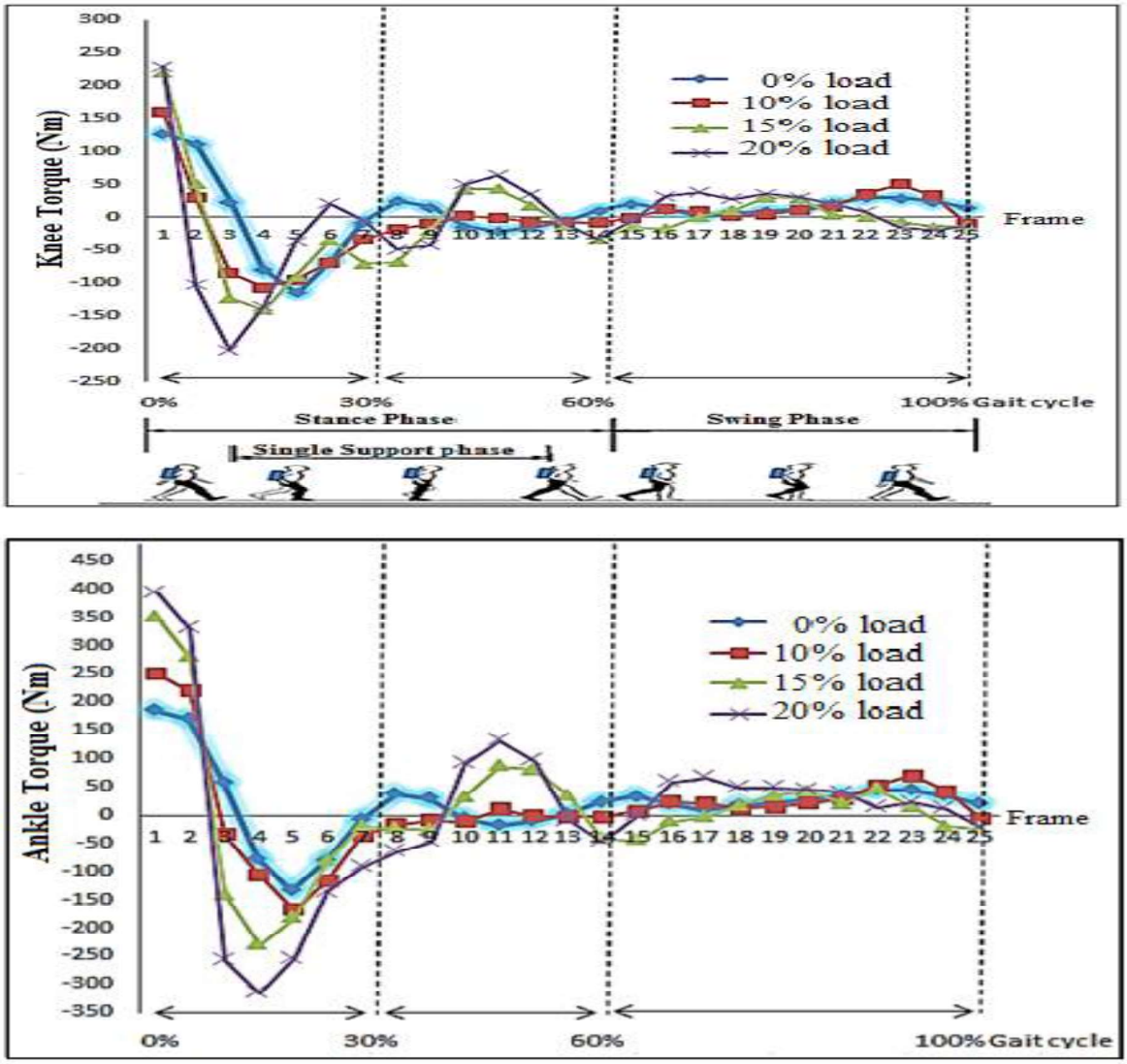

Figure 2(b): Graphs of knee torque (above) and ankle torque (below) with loadof 0% , 10%, 15%, and 20% of body weight (BW).

Next 30% gait cycle of walking, knee and ankle angles had different decrement and increment situation. While the torque values of knee and ankle made a little bit small increments and reduction in 15% and 20% load of BW. Researchers reported that knee flexion during middle stance assists to maintain stability by keeping the body's centre of mass decreased [5].

The third phase, after 60% gait cycle of walking, the knee angles graphs produced lowest minimum angle in 20% load of BW and for ankle angles graphs produced greatest angle also in 20% load of BW. The torque values of knee and ankle were nearly approached zero for all load conditions because the weight of the body was being transferred to the other foot. This is because the torques already normalized through body weight and leg length to gain stability [10].

4.0 CONCLUSION

The purposes of this study were to determine the effect of ankle and knee angle and to evaluate the values of torque at ankle and knee joint using Kane's method while walking with backpack loads of 0%, 10%, 15% and 20% of body weight. The torque at ankle and knee in lower limb play very important role to gain stability during walking either with or without the load. At the end of the study, a safe load limit for primary school children is suggested not more than 10% of body weight. Finally, musculoskeletal problems of primary school children especially at lower limb which are critical in the rapid growing age can be solved.

REFERENCES

[1] Kinoshita H. "Effect of different load and carrying systems on selected biomechanical parameters describing gait." Ergonomics, 28, (1985):1347–1362.

[2] Pascoe, D.D., Pascoe, D.E., Wang, Y.T., Shim, D.M., and Kim, C.K. "Influence of Carrying Book Bags on Gait Cycle and Posture of Youths." Ergonomics, 40(6),(1997) :631–641.

[3] HasyatunChe Nan and Azmin Sham Rambely."Lower Limb Modelling using Newton-Euler Equation."Faculty of Science and Technology, Universiti Kebangsaan Malaysia, Bangi. (2006).

[4] Ghafariet, A.S., Meghdari, A. and Vossughi, G.R. "Estimation of Human Lower Extremity Musculoskeletal Conditions During Backpack Load Carrying." Scientia Iranica, 16(5), (2009) : 451–462.

[5] Jason C. Gillette, J.C., Stevermer, C.A., Miller, R.H., Edwards, W.B., and Schwab, C.D."Lower Extremity Joint Moments During Carrying Tasks in Children, Journal of Applied Biomechanics, 28(2), (2012): 156–164.

[6] Sharifah Alwiah, A.R., Rambely, A.S., and Ahmad, R.R."A biomechanical model via Kane's equation–Solving trunk motion with load carriage", American Journal Of Scientific And Industrial Research, 2, (2011):678 – 685.

[7] Rambely, A.S., and Fazrolrozi. "A Six-Link Kinematic Chain Model OF Human Body Using Kane's Method." International Journal of Modern Physics: Conference Series, 9, (2012): 59–67.

[8] Yamaguchi, G.T. Dynamic Modelling of Musculoskeletal Motion: A Vectorised Approach for Biomechanical Analysis in Three Dimensions. New York , Springer, 2006.

[9] Winter, D.A. Biomechanics and Motor Control of Human Movement. 6th Ed. Canada: John Wiley & Sons, Inc., 2005.

[10] Tilbury-Davis, D. C. & Hooper, R.H. "The kinetic and kinematic effects of increasing load carriage upon the lower limb." Human Movement Science, 18(5), (1999) : 693–700.

A mathematical model of lower extremity joint reaction forces of school children carrying load

Nor Hidayah Zawawi[a], Sharifah Alwiah Syed Abd. Rahman[b], Norzaida Abas[c] and Jamaliah Jusoh[d]

UTM Razak School of Engineering and Advanced Technology,UniversitiTeknologi Malaysia,54100 Kuala Lumpur, Malaysia

[a]hidayah_kmb@yahoo.com, [b]shalwiah.kl@utm.my, [c]zaida.kl@utm.my, [d]syalya495@gmail.com

Abstract - *A two-dimensional model of foot segment is developed using Newton-Euler Method in this study. The objectives of this study are to obtain moments and forces at the ankle and knee joint through an inverse dynamic method. The moment and forces can be calculated based on the data produced from the experiment of a primary school children carrying different backpack load conditions: 0%, 10%, 15% and 20% of body weight. The loads are carried at the back of the body using a two-strapped backpack without waist-belt and the subjects are required to walk on a 6 metres track provided. Result shows that the maximum values of ankle and knee moment occurred in a single support phase while forces are at a maximum peak in double support phase especially for the 20% load carriage.*

Keywords: Backpack, Newton-Euler Method, Torques

1.0 INTRODUCTION

Backpack is one of the several forms of manual load carriage that provides versatility and is often used by hikers, backpackers and soldier, as well as school students [1]. However, most school children carry heavy backpacks to school everyday for a long period of time. The ideal load carrying system would be one that did not disturb the body's natural posture, balance and movements [2]. Several investigations on backpack related injuries and lower back pain have been reported. Backpacks carried by school children from kindergarten through college may be associated with some potential health consequences, including muscular aches, back strain, altered gait, bad posture and eventual low back pain. In particular, heavy backpacks can put pressure on the growing joints and ligaments of young school children, thus initiating the back strain process. One of the study on postural discomfort showed that most of the children reported the occurrence of sharp radiating pins and needle type pain [3].

A three-dimensional mathematical model of the biomechanical interactions between backpack and bearer during load carriage has been studied by Ren [4]. The model considers both the coupled pack motions, which follow the torso, and also the longitudinal compliance and damping in the backpack suspension system [4]. Carrying heavy backpack is not only effected the spine (upper limb), but also affected the lower limb of the human body. The effects of walking in high heeled shoes and

carrying load asymmetrically, on joint kinetics of lower extremity in 15 young females was investigated by Jing and Soul [5]. Results showed that hip extensor moment significantly increased with the heel height increase but not with the load weight increase. Walking in high-heeled shoes and carrying a load increased knee extensor moment and diminished ankle plantar flexor moment. When high-heeled shoes and asymmetrically carried load are combined, the changes of joint kinetics at each joint are much greater than that caused by the high-heeled or load carriage alone.

To our knowledge, there have been very few scientific studies on backpack-related problems especially on school children. Even though there was a study on backpack-related problems, most of the studies deal with adults and teenagers only. Furthermore, most of the studies do not use mathematical model to determine the effects of load carriage in term of forces and moments. Thus, this paper aims to develop a mathematical model to calculate the forces and moments acting on the lower limb during walking while carrying different load of backpack.

2.0 METHODOLOGY

Seven primary school children aged 7 to 9 years old with average weight ±29.17 kg and average height ±1.25 m participated in this study. Before the experiment, physical measurement of the school children were measured such as the weight, height, the diameter of the left and right wrists, palms thick, knee diameter and ankle diameter were recorded. Informed consent was obtained from each subject and their parents prior to the study. The experiment was done in the Movement Analysis Laboratory in University Malaya. Subjects were asked to walk on a 6 meter track provided, without carrying a backpack (0% load) and by carrying a backpack with load of 10%, 15% and 20% of their body weight. The movement were recorded using a Motion Analysis Vicon Nexus 1.5.2 system with 7 units infrared camera at 50 Hz. Each student has to do four trials of experiments for each backpack load carriage. In this paper, two segment of a lower limb model were developed using Newton-Euler Method in sagittal-plane.

2.1 Nomenclature For The Free Body Diagram

F_x, F_y = Force acting in the x-axis and y-axis

θ = Joint angle at a mass center in the horizontal axis (angular displacement)

$\dot{\theta}, \ddot{\theta}$ = angular velocity and angular acceleration at a mass center

I = moment of inertia in sagittal plane

m = mass of the body

l = distance from the connection joint to a segment mass center

M = moment of a segment

x, y = horizontal and vertical component

$\dot{x}, \dot{y}, \ddot{x}, \ddot{y}$ =linear velocity and linear acceleration on x and y-axis

M_i = total moment acting nearer to a segment i

M_{pgi} = total moment acting nearer to a center of a segment i

m_i =mass of a segment i

F_{pgi} =force acting from center of gravity of a segment i.

F_{ik} =force acting on particle i from particle k

force acting on particle i from particle k is the same as force acting on particle k from particle I, then $F_{ik} = F_{ki}. (i = 1,2,3, \ldots)$

2.2 Forces and moment acting on a two segments of a lower limb.

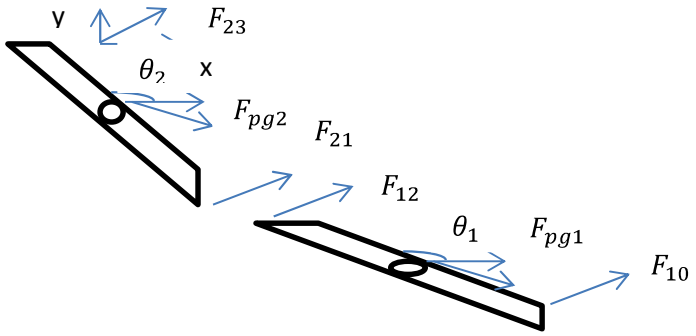

Figure 1:A Free body diagram of a rigid body model on a lower limb

Forces,
x-component of a first segment,

$$F_{10}^x + (-F_{12}^x) + F_{pg1}^x = m_1\ddot{x}_1 \quad (1)$$

x-component of a second segment,

$$F_{21}^x + (-F_{23}^x) + F_{pg2}^x = m_2\ddot{x}_2 \quad (2)$$

y-component of a first segment,

$$F_{10}^y + \left(-F_{12}^y\right) + F_{pg1}^y = m_1\ddot{y}_1 \quad (3)$$

y-component of a second segment,

$$F_{21}^y + \left(-F_{23}^y\right) + F_{pg2}^y = m_2\ddot{y}_2 \quad (4)$$

Moment of a first segment,

$$(l_{10}sin\theta_1)(F_{10}^x) + (-l_{12}sin\theta_1)(-F_{12}^x) + (l_{10}cos\theta_1)(F_{10}^y) + (l_{12}cos\theta_1)\left(-F_{12}^y\right) + M_{pg1} + M_1 - M_2 = I_1\ddot{\theta}_1 \quad (5)$$

$$(l_{21}sin\theta_2)(F_{21}^x) + (-l_{23}sin\theta_2)(-F_{23}^x) + (-l_{21}cos\theta_2)(F_{21}^y) + (l_{23}cos\theta_2)\left(-F_{23}^y\right) + M_{pg2} + M_2 - M_3 = I_2\ddot{\theta}_2 \quad (6)$$

Because of the free body diagram, the constraint of the first segment is

$$x_1 = x + l_{10}cos\theta_1 \quad (7)$$

$$y_1 = y + l_{10}sin\theta_1 \quad (8)$$

Constraint of the second segment,

$$x_2 = x + l_1cos\theta_1 + l_{21}cos\theta_2 \quad (9)$$

$$y_1 = y + l_1sin\theta_1 + l_{21}sin\theta_2 \quad (10)$$

Differentiate $x_1$and $x_2$with respect to θ gives,

$$\dot{x}_1 = \dot{x} + (-l_{10}\dot{\theta}_1 sin\theta_1) \quad (11)$$

$$\dot{x}_2 = \dot{x} + (-l_1\dot{\theta}_1 sin\theta_1) + (-l_{21}\dot{\theta}_2 sin\theta_2) \quad (12)$$

Second differentiation of $x_1$and $x_2$with respect to θ gives,

$$\ddot{x}_1 = \ddot{x} + (-l_{10}\dot{\theta}_1{}^2 cos\theta_1) + (-l_{10}\ddot{\theta}_1 sin\theta_1) \quad (13)$$

$$\ddot{x}_2 = \ddot{x} + (-l_1\dot{\theta}_1{}^2 cos\theta_1) + (-l_1\ddot{\theta}_1 sin\theta_1) + \left(-l_{21}\dot{\theta}_2{}^2 cos\theta_2\right) + (-l_{21}\ddot{\theta}_2 sin\theta_2) \quad (14)$$

Differentiate $y_1$and $y_2$with respect to θ gives,

$$\dot{y}_1 = \dot{y} + (l_{10}\dot{\theta}_1 cos\theta_1) \quad (15)$$

$$\dot{y}_2 = \dot{y} + (l_1\dot{\theta}_1 cos\theta_1) + (l_{21}\dot{\theta}_2 cos\theta_2) \quad (16)$$

Second differentiation of $y_1$and $y_2$with respect to θ gives,

$$\ddot{y}_1 = \ddot{y} + (-l_{10}\dot{\theta}_1{}^2 sin\theta_1) + (l_{10}\ddot{\theta}_1 cos\theta_1) \quad (17)$$

$$\ddot{y}_2 = \ddot{y} + (-l_1\dot{\theta}_1{}^2 sin\theta_1) + (l_1\ddot{\theta}_1 cos\theta_1) + \left(-l_{21}\dot{\theta}_2{}^2 sin\theta_2\right) + (\, l_{21}\ddot{\theta}_2 kos\theta_2) \quad (18)$$

Substitute the equation of (13) into (1) for x-component of the first segment,

$$F_{10}^x - F_{12}^x = -F_{pg1}^x + m_1\ddot{x} - m_1 l_{10}\dot{\theta}_1{}^2 cos\theta_1 - m_1 l_{10}\ddot{\theta}_1 sin\theta_1 \quad (19)$$

Substitute the equation of (14) into (2) for x-component of the second segment,

$$F_{21}^{x} - F_{23}^{x} = -F_{pg2}^{x} + m_2\ddot{x} - m_2 l_1 \dot{\theta_1}^2 cos\theta_1 - m_2 l_{21}\dot{\theta_2}^2 cos\theta_2 - m_2 l_1 \ddot{\theta}_1 sin\theta_1 - m_2 l_{21}\ddot{\theta}_2 sin\theta_2 \quad (20)$$

Substitute the equation of (17) into (3) for y-component of the first segment,

$$F_{10}^{y} - F_{12}^{y} = -F_{pg1}^{y} + m_1\ddot{y} - m_1 l_{10}\dot{\theta_1}^2 sin\theta_1 + m_1 l_{10}\ddot{\theta}_1 cos\theta_1 \quad (21)$$

Substitute the equation of (18) into (4) for y-component of the second segment,

$$F_{21}^{y} - F_{23}^{y} = -F_{pg2}^{y} + m_2\ddot{y} - m_2 l_1 \dot{\theta_1}^2 sin\theta_1 - m_2 l_{21}\dot{\theta_2}^2 sin\theta_2 + m_2 l_1 \ddot{\theta}_1 cos\theta_1 + m_2 l_{21}\ddot{\theta}_2 kos\theta_2 \quad (22)$$

Rearrange the moment equation gives,

$$(l_{10}sin\theta_1)(F_{10}^{x}) + (l_{12}sin\theta_1)(F_{12}^{x}) - (l_{10}cos\theta_1)(F_{10}^{y}) - (l_{12}cos\theta_1)\left(F_{12}^{y}\right) + M_1 - M_2 = -M_{pg1} + I_1\ddot{\theta}_1 \quad (23)$$

$$(l_{21}sin\theta_2)(F_{21}^{x}) + (l_{23}sin\theta_2)(F_{23}^{x}) - (l_{21}cos\theta_2)(F_{21}^{y}) - (l_{23}cos\theta_2)\left(F_{23}^{y}\right) + M_2 = -M_{pg2} + I_2\ddot{\theta}_2 + M_3 \quad (24)$$

Equations (19), (20), (21), (22), (23) and (24) are 6 equations with six variables, which are $F_{10}^{x}, F_{12}^{x}, F_{10}^{y}, F_{12}^{y}, M_1$and M_2. These equations can be formed in a matrix form. Given that, $F_{23}^{x} = F_{23}^{y} = M_3 = 0$. Then,

$$\begin{pmatrix} 1 & -1 & 0 & 0 & 0 & 0 \\ 0 & 1 & 0 & 0 & 0 & 0 \\ 0 & 0 & 1 & -1 & 0 & 0 \\ 0 & 0 & 0 & 1 & 0 & 0 \\ l_{10}sin\theta_1 & l_{12}sin\theta_1 & -l_{10}cos\theta_1 & -l_{12}cos\theta_1 & 1 & -1 \\ 0 & l_{21}sin\theta_2 & 0 & -l_{21}cos\theta_2 & 0 & 1 \end{pmatrix} \begin{pmatrix} F_{10}^{x} \\ F_{12}^{x} \\ F_{10}^{y} \\ F_{12}^{y} \\ M_1 \\ M_2 \end{pmatrix}$$

=

$$\begin{pmatrix} -F_{pg1}^{x} + m_1\ddot{x} - m_1 l_{10}\dot{\theta_1}^2 cos\theta_1 - m_1 l_{10}\ddot{\theta}_1 sin\theta_1 \\ -F_{pg2}^{x} + m_2\ddot{x} - m_2 l_1 \dot{\theta_1}^2 cos\theta_1 - m_2 l_{21}\dot{\theta_2}^2 cos\theta_2 - m_2 l_1 \ddot{\theta}_1 sin\theta_1 - m_2 l_{21}\ddot{\theta}_2 sin\theta_2 \\ -F_{pg1}^{y} + m_1\ddot{y} - m_1 l_{10}\dot{\theta_1}^2 sin\theta_1 + m_1 l_{10}\ddot{\theta}_1 cos\theta_1 \\ -F_{pg2}^{y} + m_2\ddot{y} - m_2 l_1 \dot{\theta_1}^2 sin\theta_1 - m_2 l_{21}\dot{\theta_2}^2 sin\theta_2 + m_2 l_1 \ddot{\theta}_1 cos\theta_1 + m_2 l_{21}\ddot{\theta}_2 kos\theta_2 \\ -M_{pg1} + I_1\ddot{\theta}_1 \\ -M_{pg2} + I_2\ddot{\theta}_2 + M_3 \end{pmatrix}$$

3.0 RESULTS AND DISCUSSION

In this study, the inverse dynamics method was employed to obtain moments and forces at the ankle and knee joint during gait in both cases of normal gait and under load carrying conditions:10%, 15% and 20% of body weight. The moment, vertical and horizontal force values have been estimated using the developed equations from the two segments model.

Based on Figure 2 and Figure 3, it can be observed that as the load increased, the values of the moment are at a maximum and minimum peak of the knee and ankle joints. The 20% load condition is at a maximum peak compared to load of 0%, 10% and 15% of body weight. From Figure 2 ankle moment shows the increment in backpack load from 0% to 10%, 15% and 20% of body weight. The increment also changed the amplitude of the ankle moment. This can be clearly seen during stance phase. Beginning with the ipsilateral foot touches the ground until after the double support, ankle moment was at dorsal flexion direction until a minimum peak in frame 5 with the minimum value of –2 Nm. However, ankle moment was at plantar flexion direction and increased rapidly during a single support upon reaching the maximum peak in frame 8. The extreme maximum peak of ankle moment occurred at 3Nm for 20% load condition. While for loads of 0%, 10% and 15% of body weight each moment is 0 Nm, –0.2 Nm and –0.5 Nm respectively.

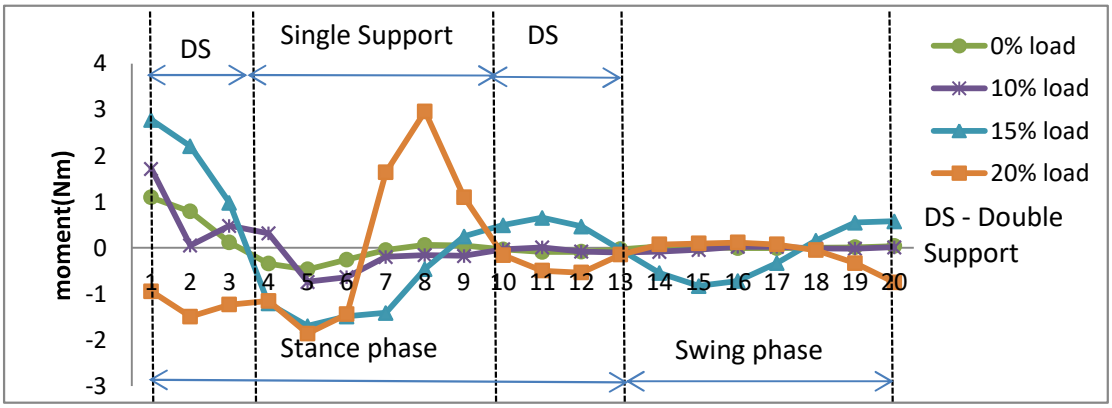

Figure 2: Ankle moment during walking with a different backpack loads

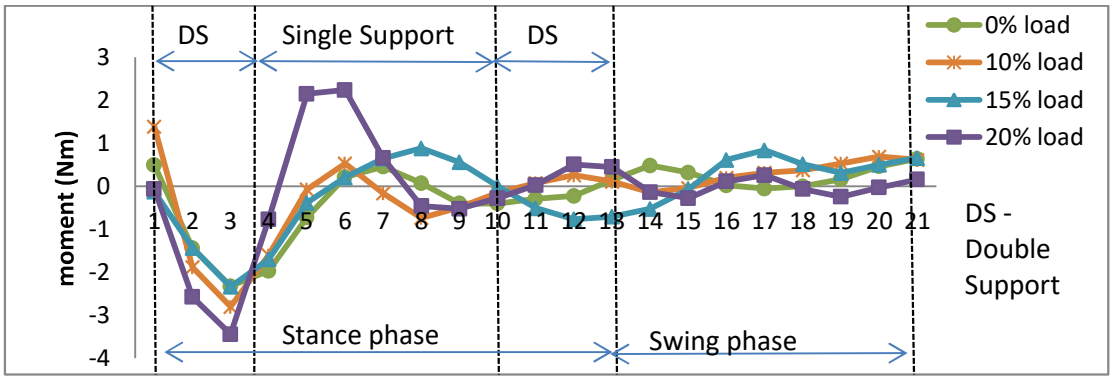

Figure 3: Knee moment during walking with a different backpack loads

From Figure 3, the increases in backpack load from 0% of body weight to 10%, 15% and 20% of body weight also change the amplitude of the knee moment. Immediately after the ipsilateral leg touching the ground, knee moment makes an extension during the gait cycle. The maximum value of knee moment occurred between frame 6 to frame 8 in a single support phase. The extreme maximum peak occurred in frame 6 with the value of 2 Nm for the 20% load condition. While for 0%, 10% and 15% of body weight each gives the value of 0.5 Nm, 0.5 Nm and 1.0 Nm respectively. When the ipsilateral leg is in the swing phase knee moment decreases until it reached a minimum peak in frame 15. The minimum value of knee moment is –0.5 Nm for the 20% load condition.

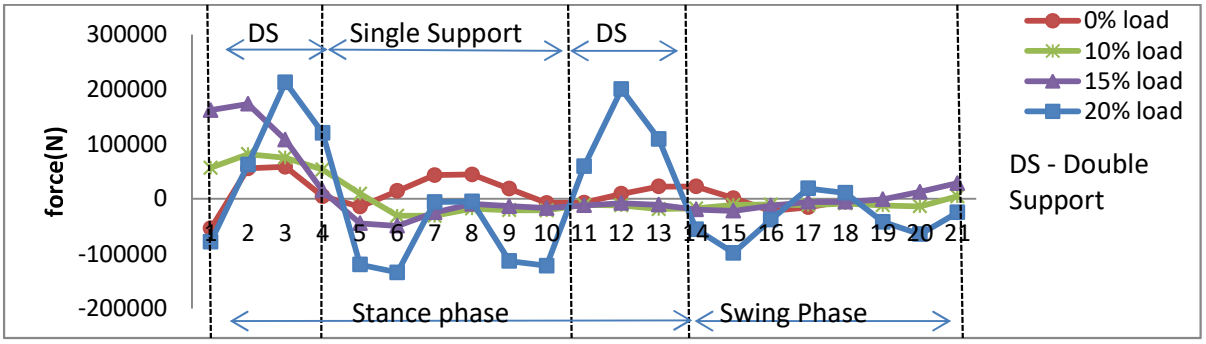

Figure 4: Ankle forces in the *x*-component

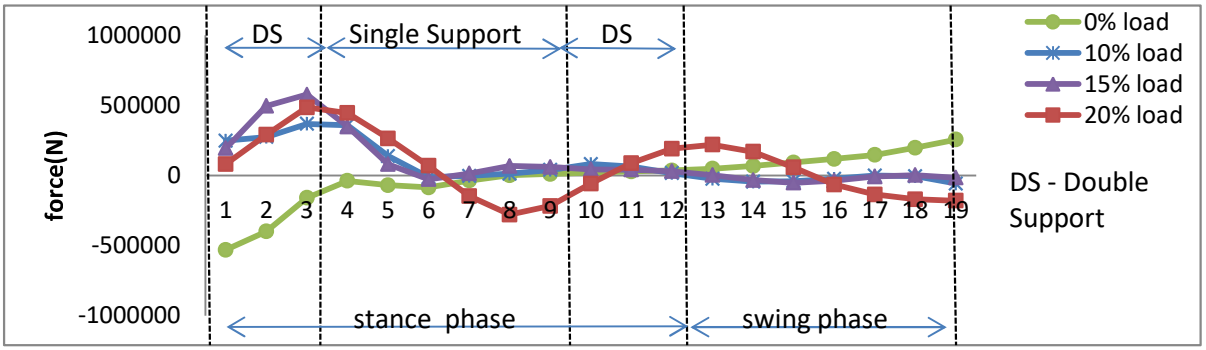

Figure 5: Ankle forces in the *y*-component

It is observed that ankle forces from the *x*-component in Figure 4 increased rapidly when ipsilateral leg touched the ground in double support phase. However, in single support phase in which only the ipsilateral leg is on the ground, the ankle forces reduced to minimum values. The extreme minimum value is when carrying the 20% load condition which occurred in frame 6 with the value of 140 000N, compared to 10% and 15% load conditions that give the values of –25000N and –50000N respectively. During the second double support, the forces increased rapidly to a maximum peak of 200 000N for 20% load condition. Ankle force is minimum in swing phase with the value of 100 000N in the negative direction for the load of 20% of body weight. The force is minimal in this phase because the burden is borne by the contralateral leg which is in a single support phase.

According to Figure 5, the forces acting in *y*–component having a dorsal flexion direction after ipsilateral heel touching the ground and having a plantar flexion

direction starting from a single support until the final stance phase. The minimum force occurred in frame 8 just before entering the double support phase. At this time, carrying the load of 20% of body weight provided the extreme minimum peak value of –300 000 N compared to 10% and 15% load conditions, each of almost 0 N and 80 000 N respectively. The force acting in the swing phase is at the minimum value of 200 000 N in the negative direction for the load of 20% of body weight.

Based on the Figure 4 and Figure 5, it can be concluded that in case of lower limb joints (ankle joint), force values in the horizontal direction are less than the force values of vertical direction. In addition, forces are at its maximum peak in double support phase especially for the 20% load condition. These show that more forces are needed to support the load when both feet are on the ground.

4.0 CONCLUSION

This paper presents a two-dimensional model of foot segment in a sagittal plane using Newton-Euler method. An inverse dynamics approach was utilized to estimate the forces and moment on the lower extremity namely the ankle and knee during backpack load carrying. Results showed that, when the ipsilateral leg is in the stance phase, the ankle forces from the x and y–component increased. While, ankle moment decreased during this phase. However, when the ipsilateral leg is in the swing phase, the ankle forces from the x and y–component decreased. While, ankle moment is increased gradually in the swing phase. In this case, the forces and moments at the lower limb are balancing and maintaining stability during gait performance while carrying backpack load.

REFERENCES

[1] Knapik, J., Harman E. and Reynolds K. “Load Carriage Using Packs: A Review of Physiological, Biomechanical and Medical Aspects.” Applied Ergonomics, 27, (3), (1996) : 207–216.

[2] Farideh Babakhani. “The effect of backpack load on the posture of children and its relationship to trunk muscle activity during walking on a treadmill.” Thesis Doctor of Philosophy, Saarland University, 2011.

[3] Avantika Rai, ShaliniAgarawal. “Back Problems Due To Heavy Backpacks in School Children”. Journal Of Humanities And Social Science, 10(6), (2013): 22–26.

[4] Ren, L., Howard, D., and Jones R.K. “Mathematical Modelling of Biomechanical Interactions between Backpack and Bearer during Load Carriage.” Journal of Applied Mathematics, 1, (2013): 1–13.

[5] Jing, X. L, and Soul L. “Joint moment of lower limbs during walking with high-heeled shoes and asymmetric load carrying in young females.” Proceeding conference of 30th Annual Conference of Biomechanics in Sports, Melbourne, 2012 : 393 – 396.

Synthesis and Structural Characterisation of Zinc Oxide Thin Film by Thermal Evaporation of Zinc Powder

Ithnaini Muhamed Kamil [1,a], Yussof Wahab[1,b], Astuty Amrin[1,c] and Rosnita Muhammad[2,d]

[1]Department of Science, Razak School of Engineering and Advanced Technology, Universiti Teknologi Malaysia, 54100 Kuala Lumpur, Malaysia
[2]Department of Physics, Faculty of Science, Universiti Teknologi Malaysia, 81310 Skudai Johor, Malaysia

[a]*ithnaini@mara.gov.my*, [b]*ybw@utm.my*, [c]*astuty@utm.my*, [d]*rosnita@utm.my*

Abstract – *The ZnO thin films are synthesized by thermal evaporation method of high purity metallic zinc powder at temperatures of 500 °C, 550 °C, 600 °C, 650 °C and 700 °C in a flow of Ar and O_2 gas mixture. Analysis on its morphology, phase composition and crystallinity of the structures are carried out using X-ray diffraction (XRD), Field Emission Scanning Electron Microscope (FESEM) and Atomic Force Microscope (AFM). Two samples at temperatures of 500 °C and 600 °C are then post annealed to temperatures of 800 °C and 900 °C. The structural analysis is then carried out using FESEM and XRD to compare the results of before and after the post annealing. The size of the diameter of the structures growth depends on the temperatures of the substrate but a significant pattern could not be determined. The structure of the ZnO also changes from wires/rods to flower as it reached temperature of 700 °C. The optimum temperature to grow ZnO on a glass substrate using thermal evaporation method was concluded at 650 °C. The XRD patterns revealed that wires grown are vertically to the substrate with preference of intense peaks are observed along (002) directions.*

Keywords: Zinc Oxide, Thermal Evaporation, X-ray Diffraction (XRD), Field Emission Scanning Electron Microscope (FESEM), Atomic Force Microscope (AFM)

1.0 INTRODUCTION

Nanostructure materials are currently being studied by many research groups due to its quantum confinement effect and enhanced surface states. Zinc oxide, ZnO at nanoscale can be represented with various morphologies such as nanowires, nanorods, nanobelts, nanotubes nanoflowers and nanoplates. ZnO is an n-type metal oxide material with large direct band gap of ~3.3 eV at room temperature and large exciton binding energy of 60 meV compared to GaN (25 meV) and ZnSe (26 meV) with high melting point of 1975 °C making it a stable exciton-related UV emitter and as a choice of material to be used in multi-application areas [1]. These characteristics contribute to higher breakdown voltages, ability to sustain large electric fields, lower electronic noise and high temperature and high power operation [2]. Its low cost and

efficient excitonic emission in comparison to other semiconductor materials ensuring it for large scale optoelectronic applications.

ZnO is a hexagonal wurtzite crystalline structure. It is most stable at ambient conditions and consist of 2 lattice parameters, known as a and c. For an ideal hcp structure, the ratio of c/a is 1.633. Each Zn ion is surrounded by 4 O ions at the corners of tetrahedron. The structure may become zinc-blende or rocksalt structure at relatively high pressure. The synthesis of ZnO can be done either at high temperature vapor phase processes or at low temperature solution routes [3]. Higher temperature produces high quality of ZnO growth using expensive substrates such as sapphire. The low temperature method is chosen due to its simplicity and low cost. High quality ZnO films were produced by thermal oxidation of metallic Zn thin films [4]. It is also reported that an average diameter of 40 nm ZnO were synthesized by thermal oxidation in suitable oxygen atmosphere by heating the Zn powder directly [5]. Work also done on the effect of oxygen flow using thermal evaporation method on the synthesized of ZnO nanorods on Si (100) and sapphire (0001) substrates [6]. Previous research also indicate that the gas flow rate and oxygen content during layer deposition using thermal evaporation method strongly influence the morphology of ZnO nanostructures at temperature of 390 °C [7]. In this work, thermal evaporation method which is simple and cost effective is chosen as a way to synthesis the ZnO wires with soda lime glass as the substrate having the thickness of 1 mm at temperatures of 500 °C, 550 °C, 600 °C, 650 °C and 700 °C.

2.0 METHODOLOGY

2.1 Synthesis of ZnO Wires

The thermal evaporation was done in horizontal quartz Thermolyne F21100 Tube Furnace. The apparatus used are the lumina boat, substrate holder, soda lime glass and tungsten bar. They were first immersed in propanol liquid which is then replaced with distilled water. Later, all the apparatus were placed inside the 3510 Branson ultrasonic cleaner with deionized water for 15 minutes. Once it is dried, 1 g of Zn powder was put into the lumina boat.

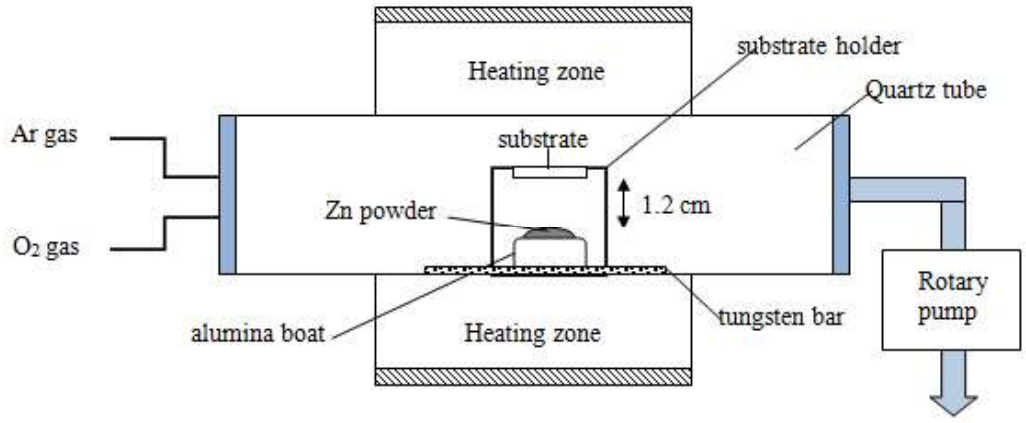

Figure 1: Schematic diagram of the experimental setup using thermal evaporation method

The gas outlet was turned on together with the vacuum pump and the temperature was set up to the desired temperature. The argon gas was let in through the gas inlet. When the temperature was nearly to the desired temperature, the oxygen tube was turned on. All gas flows were controlled by mass flow meters controllers. The argon gas functions as a carrier gas that will direct the evaporated zinc powder to the glass substrate. The oxygen will then react with the zinc and becomes zinc oxide. The ratio of the argon and oxygen was 80:20 and when observed at the pressure meter, the argon was at 1.36 psig and oxygen was at 0.34 psig. The growth time was set to ninety minutes before terminating the oxygen flow. The cooling of the samples was let to be at room temperature for at least 3 hours. 5 samples were made at temperatures of substrates at 500 °C, 550 °C, 600 °C, 650 °C and 700 °C, controlled by a thermocouple.

2.2 Post Annealing of Samples

Two samples at temperatures of 500 °C and 600 °C were then post annealed using Furnace Carbolite cwf1100. The sample of 500 °C was annealed until 900 °C while the sample of 600 °C was annealed until 800 °C. Both of the samples were then analysed using FESEM and XRD.

3.0 RESULTS AND DISCUSSION

The images of ZnO wires growth analysed by FESEM Jeol JSM-7800F Prime are shown in Figure 2. The growth of the wires is vertically on the substrate with an average length up to 14 μm. The top view shows that the wires having a hexagonal cross section. These are true for temperatures of 550 °C until 650 °C. As the temperature increases, the diameter of the wires becomes smaller. At 650 °C, the diameter of the wires can achieve 216 nm compared at 550 °C, its diameter is 286 nm. However, at temperature 700 °C, the structure of the ZnO becomes flower like. The insets of Figure 2 show the top view of the structure.

Figure 3 shows the high magnification FESEM images of ZnO structure at 700 °C that reveals its cross section can achieve 127 nm.

The FESEM images for the post annealed samples are shown in Figure 4 that indicates the diameter of the wires increases. At 800 °C, the diameter is ~696 nm and at 900 °C the diameter is ~0.82 μm.

XRD measurements were carried out to verify the orientation growth of ZnO of the samples. The major peak for each temperature can be indexed to the (002).

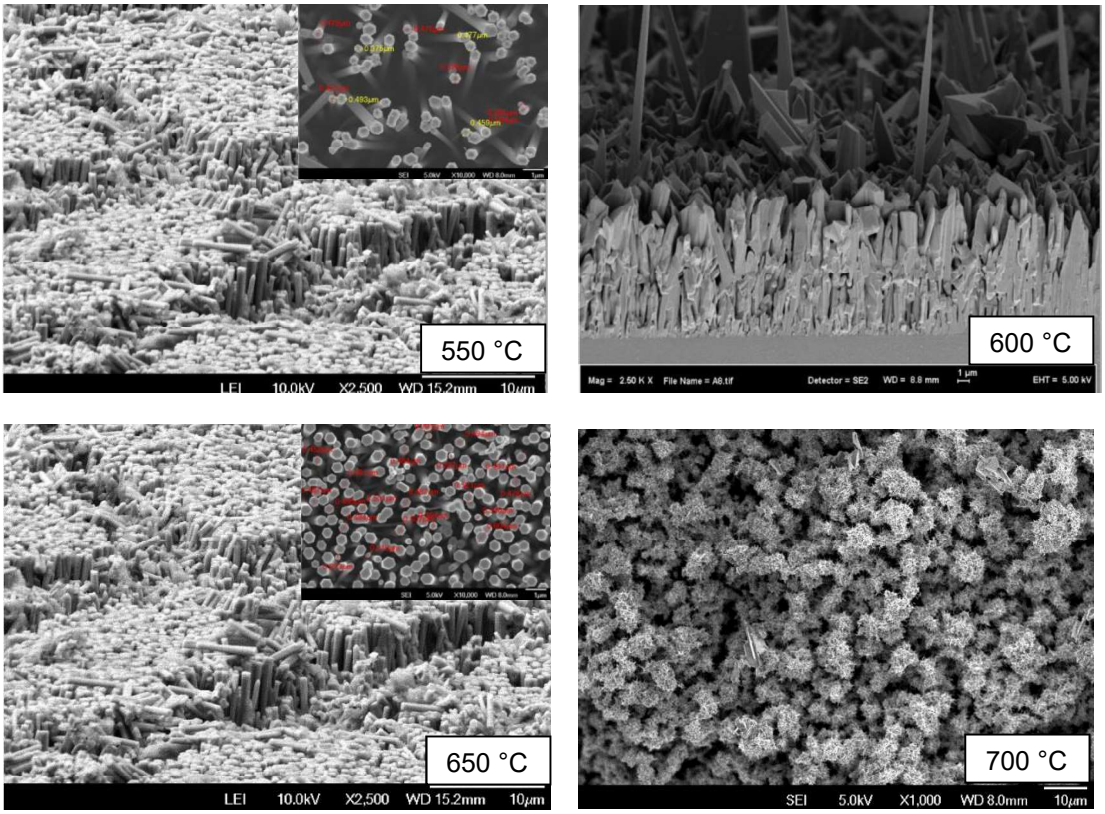

Figure 2: FESEM images of ZnO wires growth at different temperatures

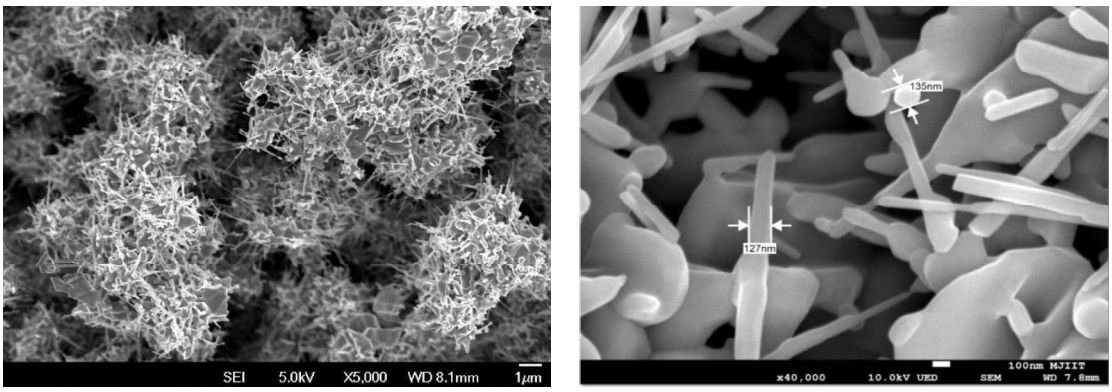

Figure 3: High magnification FESEM images at 700 °C

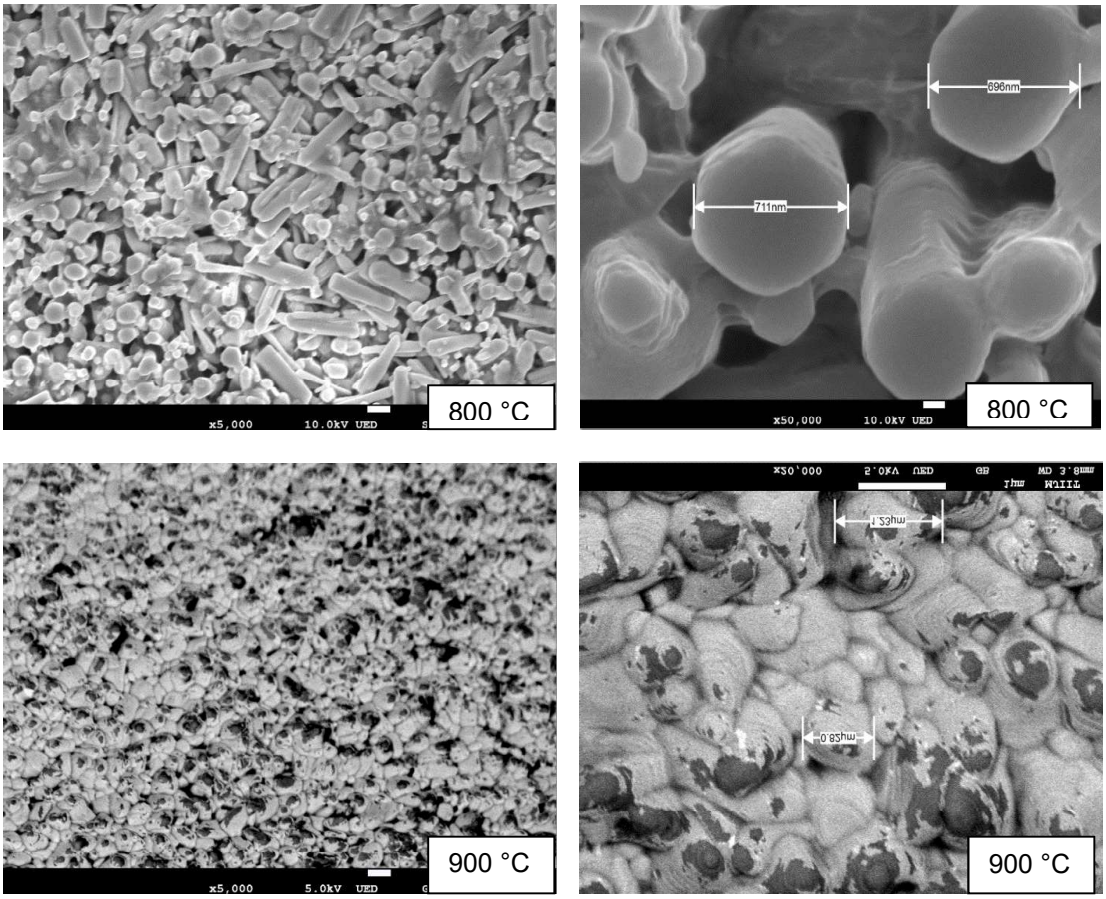

Figure 4: FESEM images for post annealed samples

The XRD patterns using PANalytical (Empyrean) apparatus with Cu-Kα 1.54060 radiation concluded that ZnO is a hexagonal wurtzite crystalline structure in accordance to PDF 01-070-8070 and PDF 01-077-9355. The 2θ range used in XD measurements was from 20° to 80°. The intensities of the peak indicating strong preferential orientation along specific c-axis crystal plane. Sharp diffraction peaks at temperatures from 550 °C until 650 °C with full width at half-maximum (FWHM) intensity indicate excellent crystal quality. The post annealed sample at 800 °C has the highest intensity also indicating the crystal quality due to heating process. The XRD pattern at 500 °C exhibit random orientation and is believed due to Zn which shows that the sample also contains Zn material that are not fully evaporated. As for the XRD pattern of the post annealed at temperature of 900 °C, it was thought that the results are probably due to the deformation of the glass substrate. No peaks from impurities such as Zn are detected in patterns from (b) to (d) in Figure 5 indicating the samples are of high purity.

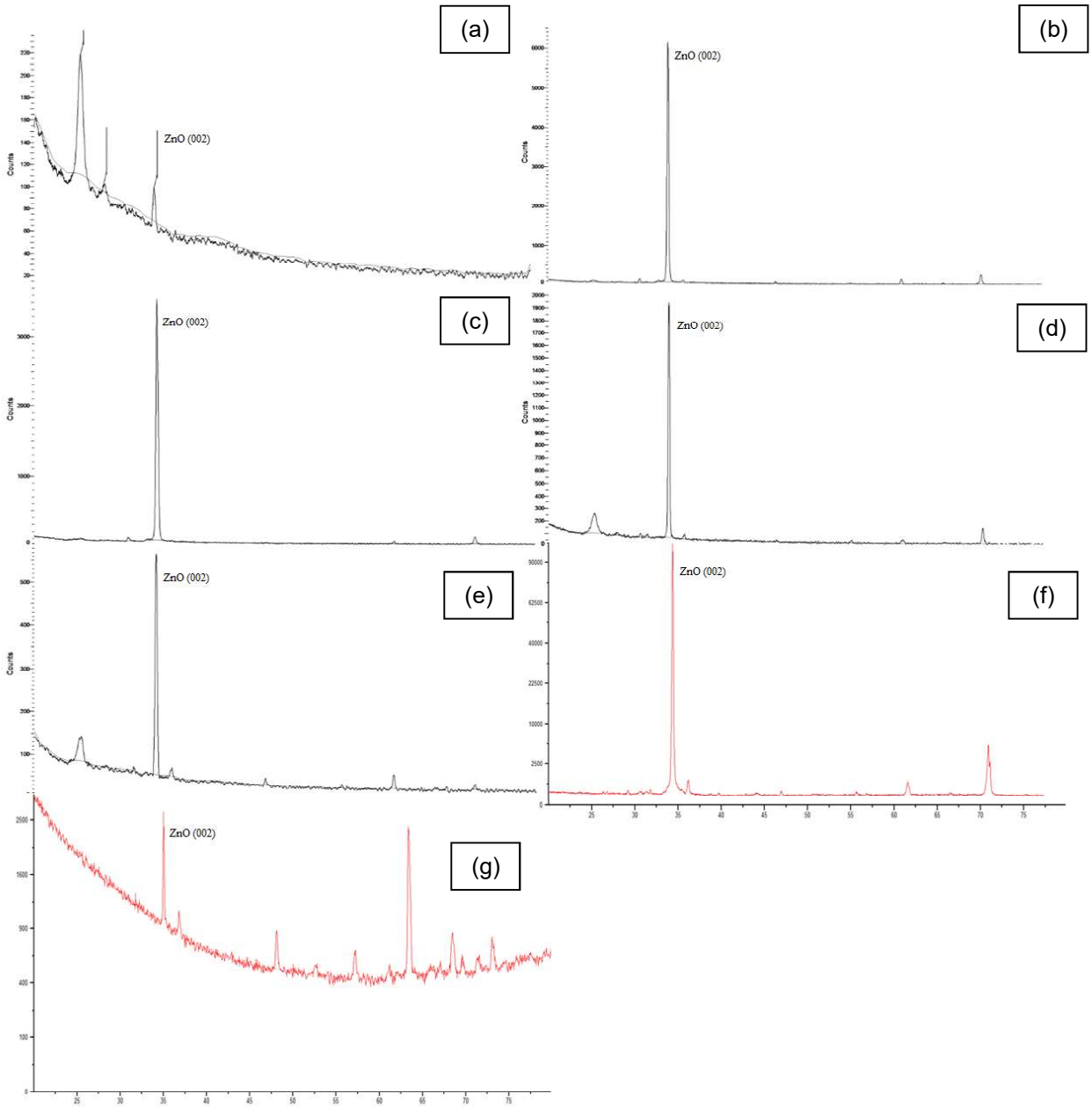

Figure 5: XRD patterns of (a) 500 °C (b) 550 °C (c) 600 °C (d) 650 °C (e) 700 °C (f) post annealed sample at 800 °C and (g) post annealed sample at 900 °C

The average grain size of ZnO nanoparticle is obtained using Scherrer's formula for crystallite size broadening of diffraction peaks:

$$D = \frac{0.9\lambda}{(\beta \cos \theta)} \quad (1)$$

Where λ is the X-ray wavelength, θ is the Bragg diffraction angle and β is the full width at half-maximum intensity (FWHM) of the diffraction peak [4]. Table 1 shows the prominent peak phase and the average grain size.

Table 1: Summarised of values obtained from XRD

T / ° C	Peak	2θ / degree	d value	Grain size / nm
500	1	25.579	3.47974	6.26
550	3	34.532	2.59528	32.20
600	2	34.727	2.58118	24.16
650	4	34.563	2.59305	31.05
700	2	34.597	2.59056	27.17
800	1	*34.941*	*2.56795*	*48.59*
900	1	*35.014*	*2.56274*	*41.73*

Analysis done by AFM reveals the morphology of the growth of ZnO. Sample at temperature 500 °C looks small in terms of size which is proven by the calculation (Table 1). It is also observed that at 650 °C, the morphology of the sample is smooth when compared to other samples at different temperatures. From the calculation obtained also, the post annealed sample shows bigger grain size as proved by FESEM image (Figure 4). However, based on the XRD patterns the intensity of the post annealed sample is higher indicating that improvement in the crystalline film quality.

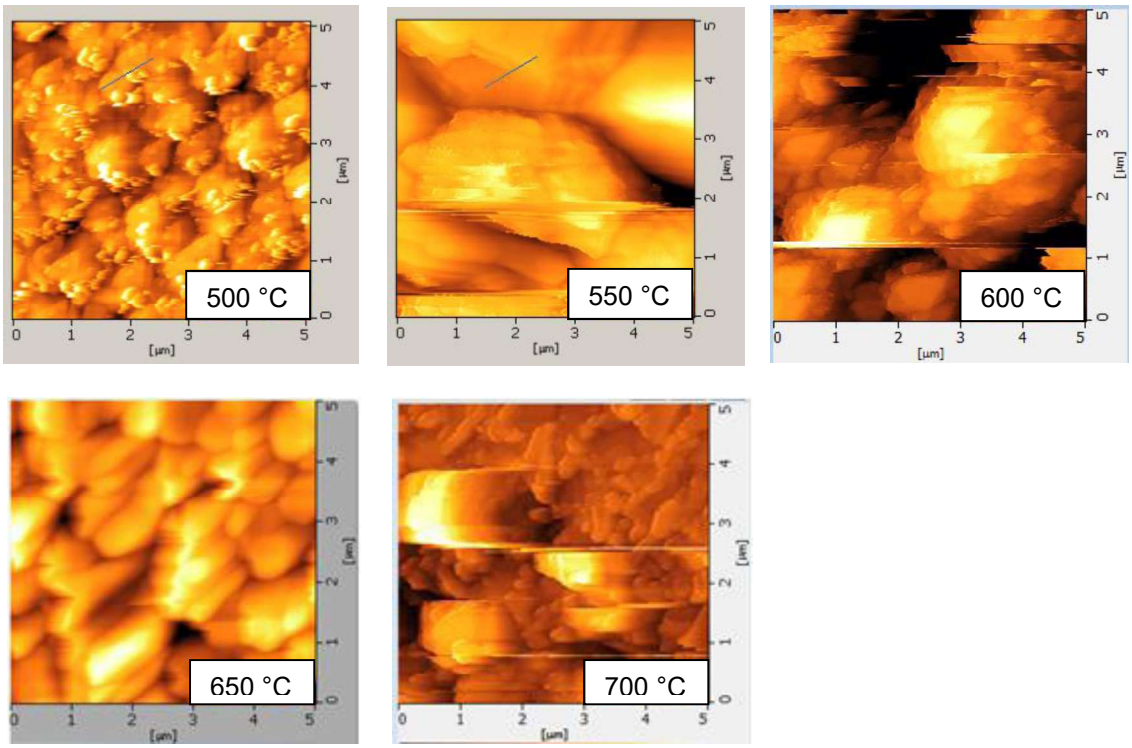

Figure 6: Images from AFM at different temperatures

4.0 CONCLUSION

The synthesis of high purity metallic zinc powder by thermal evaporation method of zinc oxide thin films at temperatures ranging between 500 °C until 700 °C were successfully carried out. Its characterization done by using FESEM, AFM and XRD revealed that as the temperatures increases, the wires show better orientation. However, the structure of the ZnO changes as the temperature approaching 700 °C from wires/rods to flower. The diameter of the wires depends on the temperatures but it does not show significant pattern. When 2 samples were post annealed to temperatures of 800 °C and 900 °C, the diameter of the wires becomes larger. Temperature at 650 °C is believed to be the optimum temperature to grow ZnO wires using thermal evaporation method as analysis done showed smooth morphology with 200 – 600 nm in diameter and having an excellent crystal quality.

REFERENCES

[1] F. Dehghan Nayeri, E. Asl Soleimani and Salehi. "Synthesis and characterisation of ZnO nanowires grown on different seed layers: The application for dye-sensitized solar cells." Renewable energy 60, (2013): 246-255.

[2] U. Özgur, Alivov, I. Ya, C. Liu, A. Teke, M. A. Reshchikov, S. Dogan, V. Avrutin, S. J. Cho and H. Morkoc. "A comprehensive review of ZnO materials and devices." Journal of applied Physics 98, no. 4 (2005): 782-803.

[3] Jingbiao Cui. "Zinc oxide nanowires." Materials characterisation 64, (2012): 43-52.

[4] S. Cho, J. Ma, Y. Kim, Y. Sun, G. K. L. Wong and J. B. Ketterson. "Photoluminescence and ultraviolet lasing of polycrystalline ZnO thin films prepared by the oxidation of the metallic Zn." Appl. Phys. Lett 75, (1999): 2761-2763.

[5] H.Y. Dang, J. Wang and S.S. Fan. "The synthesis of metal oxides nanowires by directly heating metal samples in appropriate oxygen atmospheres." Nanotechnology 14, (2003): 738-741.

[6] K. M. K. Srivatsa and D. Chhikara. "Synthesis of aligned ZnO nanorod array on silicon and sapphire substrate by thermal evaporation technique." J. Mater. Sci. Technol. 27, (2011): 701-706.

[7] S. Kitova, I. Kalaglarski, R. Stoimenov, R. Kazakov and V. Mankov. "Zinc oxide nanostructures prepared on glass substrates by thermal evaporation of zinc at atmospheric pressure." Bulgarian Chemical Communications. 45, (2013): 99-104.

[8] C. Chen, B. Yu, J. Liu, Q. Dai and Y. Zhu. "Investigation of ZnO films on Si(111) substrate grown by low energy O^+ assisted pulse laser deposited technology." J Mater Lett, (2007): 2961-2965.

[9] Zhiyong Zhang, Yuanyuan Lv, Junfeng Yan, Dandan Hui, Jiangni Yun, Chunxue Zhai and Wu Zhao. "Uniform ZnO nanowire arrays: hydrothermal synthesis, formation mechanism and field emission performance." Journal of alloys and compounds 650, (2015): 374-380.

[10] Bhagaban Behera and Sudhir Chandra. "Synthesis and characterisation of ZnO nanowires and ZnO-CuO nanoflakes from sputter-deposited brass ($Cu_{0.65}$ -

$Zn_{0.35}$) film and their application in gas sensing." Journal of materials science & technology 31, (2015): 1069-1078.

[11] Sergio Roso, Frank Guell, paulina R. Martinez-Alanis and Atsushi Urakawa. "Synthesis of ZnO nanowires and impacts of their orientation and defects on their gas sensing properties." Sensors and actuators B 230, (2016): 109-114.

[12] Muhammad Habib, Syed Sajjad Hussain, Saira Riaz and Shahzad Naseem. "Preparation and characterisation of ZnO nanowires and their applications in CO_2 gas sensors." Materials today: Proceeding 2, (2015): 5714-5719.

[13] G. A. Cuellar Murillo, C. D. Bojorge, E. A. Heredia and N. E. Walsoe de Reca. "Study of the substrate influence in ZnO nanowires oriented growth." Procedia material science 8, (2015): 630-634.

[14] Weiliang Feng, Pei Huang and Lifeng Jiang. "Preparation of highly ordered ZnO nanowire arrays by paired-cell deposition." Ceramics international 40, (2014): 6383-6387.

[15] Khyati Gautam, Inderpreet Singh, P.K. Bhatnagar and Koteswara Rao Peta. "The effect of growth temperature of seed layer on the structural and optical properties of ZnO nanorods." Superlattices and Microstructures 93, (2016): 101-108.

[16] Gang Meng, Xiaodong Fang, Weiwei Dong, Ruhua Tao, Yiping Zhao, Zanhong Deng, Shu Zhou, Jingzhen Shao and Laiang Li. "One step synthesis of vertically aligned ZnO nanowire arrays with tunable length." Applied surface science 256, (2010): 6543-6549.

[17] Nur kicir, Tunc Tuken, Ozge Erken, Cebrail Gumus and Yuksel Ufuktepe. "Nanostructured ZnO films in forms of rod, plate and flower: electrodeposition mechanisms and characterisation." Applied surface science 377, (2016): 191-199.

[18] J. Y. Chen, C. J. Pan, F.C. Tsao, C. H. Kuo, G.C. Chi, B. J. Pong, C. Y. Chang, D. P. Norton and S. J. Pearton. "Characterisation of ZnO nanowires grown on Si(100) with and without Au catalyst." Vacuum 83, (2009): 1076-1079.

Photoluminescence Of Thin Film Chalcopyrite Material $CuGaSe_2$:Zn

Azni Aziz[a] and Sathiabama Thirugnana[b]

Razak School of Engineering and Advanced Technology, Universiti Teknologi Malaysia, 54100 Jalan Sultan Yahya Petra, Kuala Lumpur, Malaysia

[a]azni@mrsmlgg.edu.my, [b]sathiabama@utm.my

Abstract – *Thin film copper with chalcopyrite structure, $CuGaSe_2$ (CGS) and $CuInSe_2$ (CIS), have attracted a big attention of many researchers as a potential, low - cost material for solar cell application. CGS has a wider energy gap of 1.68eV and its high optical absorption coefficient makes it suitable for single cells in high voltage and for top cells in tandem systems. In comparison with CGS, CIS has a narrower energy gap, 1.04 eV and a lower optical absorption coefficient. This compound semiconductor material is also a good candidate for the formation of p-n hetero-junction with a II-VI group semiconductor, because both compounds have a similar structure. One way to improve the efficiency of a $CuGaSe_2$ solar cell is to diversify its p - type to an n - type solar cell. N - type solar cell can be achieved by reducing the concentration of shallow acceptor (Cu vacancy, V_{Cu}) or by extrinsic doping. In this research the $CuGaSe_2$ material was doped with Zinc, and its optical properties and n-type conductivity of $CuGaSe_2$ for homo-junction devices were studied. The CGS material is fabricated and doping process with zinc is done by using Molecular beam Epitaxy (MBE) method. Three different concentrations of zinc were used, which are 1.2×10^{-8} cm^{-3}, 4.0×10^{-7} cm^{-3} and 9.1×10^{-7} cm^{3}, respectively. Photoluminescence measurement at room temperature shows three exciton peaks A, B and C.*

Keywords: CGS; Solar Cell, Photoluminescence, MBE, P-type, N-type

1.0 INTRODUCTION

Nowadays, the world is faced with a limited supply of non-renewable natural resources and therefore an energy crisis. The non-renewable natural resources decrease as the demand for them increases. In order to overcome this issue, scientists and researchers keep on researching and studying renewable natural resources as alternative sources of energy.

There are many renewable natural sources of energy such as wind, tidal, geothermal and solar energy which can be used as alternative sources to generate power. Sources based on solar or photovoltaic technology have become the most promising and rapidly developed for the field of the global climate challenge and alternative renewable, green and clean energy.

The world-wide market for photovoltaic technology has grown vastly in the last few years. There are many types of solar cells such as silicon solar cell, plastic or polymer solar cells, multiple junction GaAs thin film solar cell and chalcopyrite thin film solar

cell. A chalcopyrite material is found to be a potential applicant for photovoltaic and leading technologies for solar energy generation in terms of efficiency which is about 20%, the highest among thin-film devices.

Thin film copper related materials with a chalcopyrite structure, such as $CuGaSe_2$ (CGS) and $CuInSe_2$ (CIS) have attracted attention from many researchers as a potential, low cost material for solar cell application. CGS has a larger energy gap of 1.68 eV and high optical absorption coefficient which makes it a suitable material for single cells in high voltage and for top cells in tandem systems [1]. In comparison with CGS, CIS has a lower energy gap, 1.04 eV and lower optical absorption coefficient.CGS has a carrier lifetime of about 10 ps [2] while CIS is reported to be 33 ps at 8.5 K [3].

Ternary chalcopyrite semiconductors have great potential application when it comes to areas of light emitting diodes, non-linear optics, photovoltaic devices and solar cells. The solid solution of this semiconductor has been used in electro-optics devices. It also has been used for the fabrication of detectors, lasers and integrated optic devices such as modulators, filters, switches etc. In this study, we are interested on fabricating CGS:Zn, which could contribute to n-type conductivity and spark new application of chalcopyrite and solar cell materials. We also report on the photoluminescence measurement at room temperature.

2.0 METHODOLOGY

A stoichiometry CGS single crystal, and Zn doped layer are grown on GaAs substrate by a deposition sequence of migration enhanced epitaxy (MEE) [4]. We have confirmed that even at temperatures as low as 530 ^{o}C, Ga diffusion occurs prominently. GaAs is chosen as a substrate because their lattice mismatch is close to each other, less than 0.7%. The small lattice mismatch between GaAs and $CuGaSe_2$ will produced a good quality of CGS thin film.

CGS is made by alternating pilling up of layers composed of Cu and Ga atoms and Se atoms in the [001] direction. The deposition sequence starts with simultaneous deposition of Cu and Ga atoms followed by Se atom deposition. Zn doping has been done during the Cu and Ga deposition sequence of MEE to incorporate Zn to Ga lattice sites. Zn doping have three different amounts of atom concentration, 1.2×10^{-8} cm^{-3}, 4.0×10^{-7} cm^{-3} and 9.1×10^{-7} cm^{-3}.

In photoluminescence (PL) measurement, a xenon lamp tuned to 514 nm wavelength was used as an optical source. The laser beam was focused onto the samples and detected using a photodiode. For low temperature PL measurement, a nitrogen cryostat is used.PL is one of the great tools to assess the optical properties of material, such as to determine defect states and the quality of the material. When a photon with high energy compared to the band gap of a semiconductor material strikes on the semiconductor, it will cause the optical transition to take place. PL can measure physical and chemical properties of materials by using photons to induce excited electronic states in the material system and can analyse the optical emission at relaxed states. Light is directed onto the sample for excitation and the emitted luminescence is collected by a lens and passed through an optical spectrometer onto a photon detector. The spectral distribution and time dependence of the emission are related to electronic

transition probabilities within the sample. It can be used to provide qualitative and sometimes quantitative information about chemical composition, structure, impurities, kinetic process and energy transfer. PL techniques are very sensitive and only allow very small quantities (nanograms) or low concentrations (parts-per-trillion) of material to be analysed.

3.0 RESULTS AND DISCUSSION

3.1 Photoluminescence Measurement at Room Temperature

At room temperature measurement, three emission peaks are observed. Peaks which are visible during the measurement result from the emission of the photon or the recombination process when samples are exposed to light energy greater or equal than their bandgap. The results of room temperature measurement are as below.

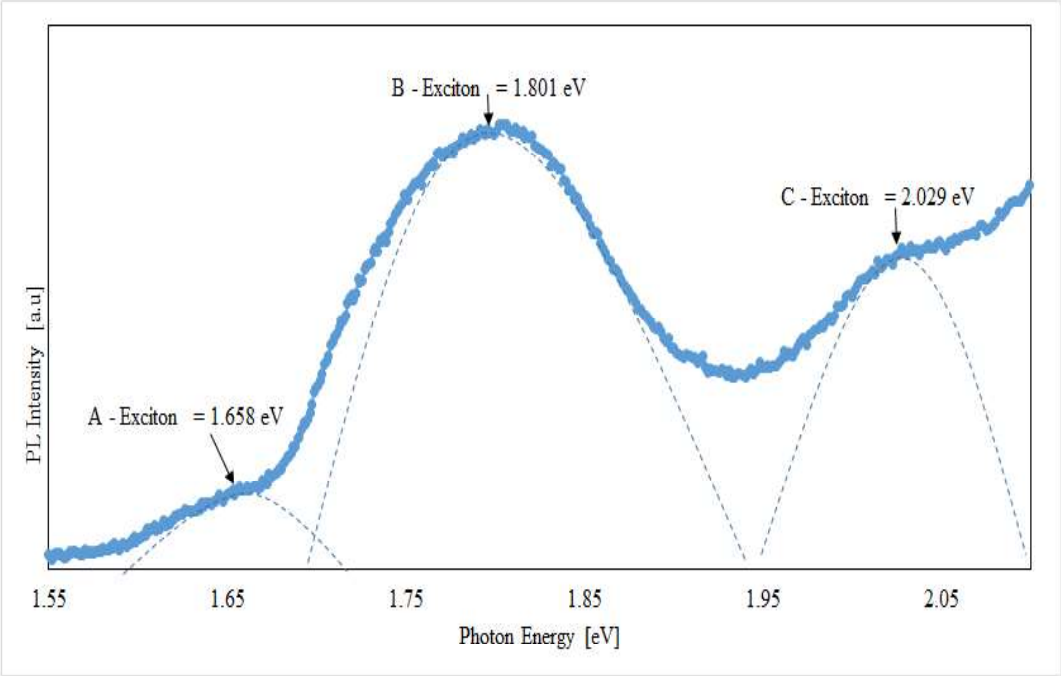

Figure 1: PL spectra of sample A at room temperature

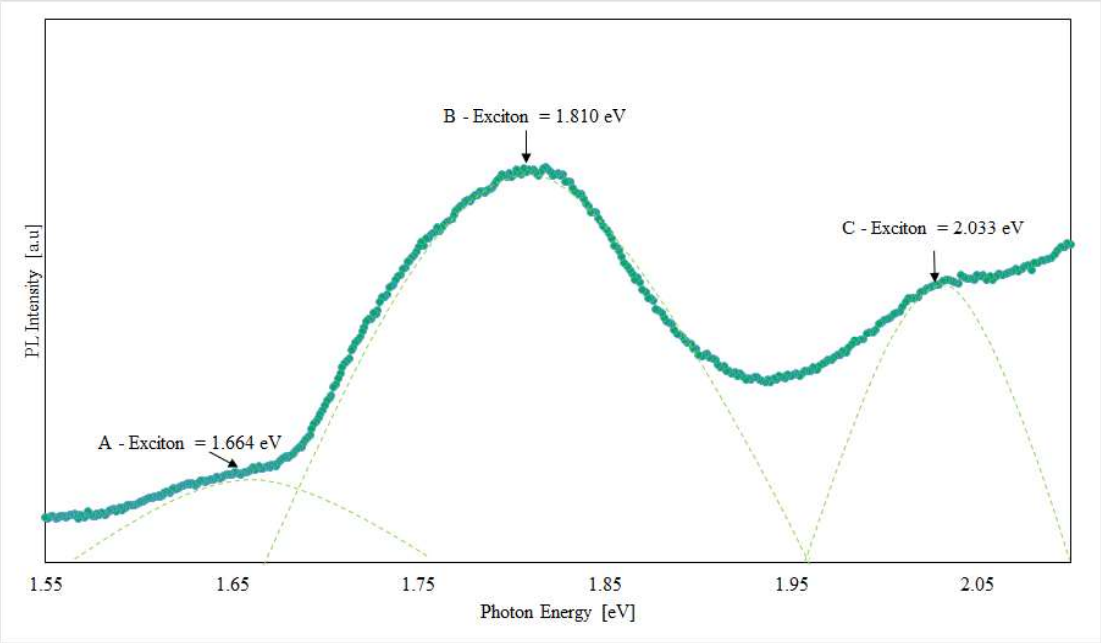

Figure 2: PL spectra of sample B at room temperature

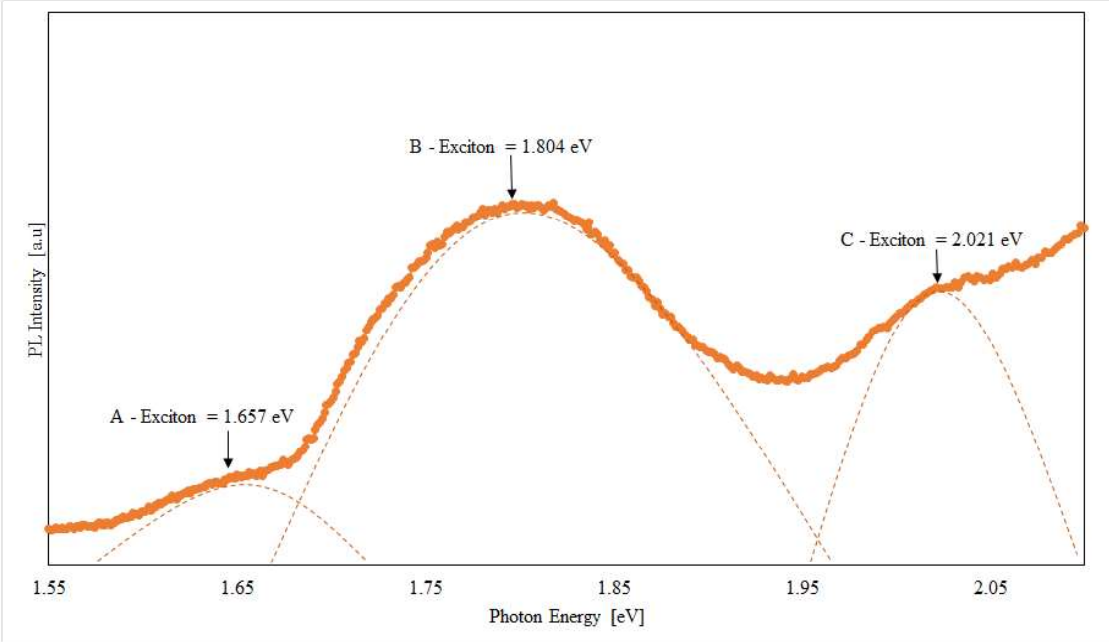

Figure 3: PL spectra of sample 3 at room temperature

Based on figures 1, 2 and 3, we can see three peaks in the PL spectrum. There is A - exciton, B - exciton and C - exciton. All these three samples show the same photoluminescence (PL) spectrum. The PL spectrums are asymmetrical and broad with shoulder peaks at the right and left sides of the graph. For sample A, A – exciton is at 1.659 eV, B - exciton at 1.801 eV and C – exciton at 2.029 eV. For sample B and C, A – exciton are 1.666 eV and 1.663 eV while for B – exciton the values are 1.810 eV and 1.804 eV, and C – exciton are 2.033 eV and 2.021 eV, respectively.

All samples show A - exciton, B - exciton and C - exciton peak. For these 3 samples, A – exciton differs in range of 1 meV – 6 meV and B – exciton differs in range 1 meV – 6 meV. The energy band of CGS is a combination of crystal – field splitting, spin orbit interactions and the valence band. [5]. Copper (Cu) plays an important role in the determination of band structures and will cause the valence band to split into three transitions A, B and C. Energies for these three transitions are A = 1.729 eV, B = 1.813 eV and C = 2.016 eV. [6]. It is almost the same as this study's values. All three samples show high dominant peak values and show all three transition levels, indicating that these samples are high quality and have high purity crystal.

The dominant peak 1.81 eV was determined in stoichiometric $CuGaSe_2$ thin film [7]. For $CuGaSe_2$ single crystal grown on GaAs the A- exciton and B-exciton are 1.713 eV and 1.71 eV due to tensile strain in the films. [8].This measurement shows the values for A- exciton and B – exciton is larger than in [8].

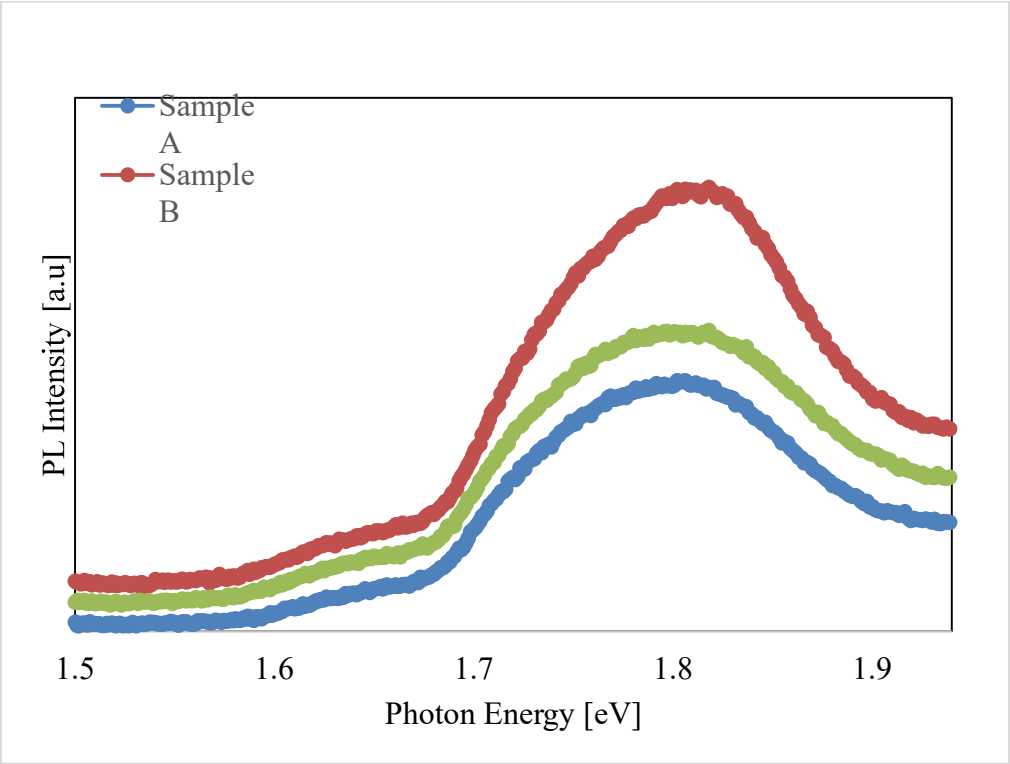

Figure 4: graph of PL Intensity [a.u] against Photon Energy [eV] for sample A, sample B and sample C at room temperature.

Figure 4 shows the comparison between these three samples. There are slight differences in the dominant peaks of these three samples. Sample B has the highest A – exciton followed by sample A and sample C. For B - exciton, sample B also has the highest value compared to sample C and sample A. For C – exciton value, sample B also has a higher value than sample C and sample A. The difference in the peak value is reliant on the amount of dopant concentration in each sample.

The results of this experiment compared with [9], the value of A - exciton in these samples is slightly lower than undoped CGS material because zinc has been doped in this samples. At the lower energy part of the spectrum, no emission is detected and it

shows that the materials are highly pure and have high crystal quality. All these samples have good potential as an absorber for photo voltaic cells because the value of A – exciton is lower and still in the practical range of energy gap for a solar cell.

Table 4.1 PL spectra of CGS:Zn at room temperature

Exciton State	A [eV]	B [eV]	C [eV]
Sample A	1.658	1.801	2.029
Sample B	1.664	1.810	2.033
Sample C	1.657	1.804	2.021

Exciton at energies higher than the basic band gap of CGS is determined through workings by [5]. In this working, all three samples show three exciton series A, B, and C. These three transitions formed because the triple valence band had split due to spin – orbit and crystal field interactions [5]. The interaction between holes and electrons from Γ6 bands lends to produce excitons with ground states or Γ1, Γ2 and Γ5 symmetries. Group [5] has observed free exciton series with n = 1 and 2 in CGS using PL.

4.0 CONCLUSION

We have successfully grown CGS:Zn samples which have high purity and high crystal quality because no noticeable emission is observed in the lower energy region at room temperature. From this result, it is confirmed that MBE growth technique is a good method to prepare a thin film chalcopyrite, because photoluminescence results at room temperature show no emission line in lower region energy which contributed to the high purity and high crystal of this material. The clear peak emission also shows that this is a good quality material.

Zinc element from group II is doped into CGS in order to improve the material's performance and to produce n- type conductivity. Three different amounts of zinc concentration were used in this study. Sample A has a zinc concentration = 1.2×10^{-8} cm^{-3}, sample B with zinc concentration = 4.0×10^{-7} cm^{-3} and sample C has a zinc concentration = 9.1×10^{-7} cm^{-3}. Zinc is chosen as a dopant material because it has the same atomic lattice as CGS and it can replace gallium site in the lattice. Zinc also shows amphoteric properties meaning it can be a donor or acceptor, same as selenium. Zinc has amphoteric properties so it can occupy the Cu lattice site (II_{Cu}, donor) or Ga site (II_{Ga}, acceptor) [10]. Doping must be done in order to change and increase the conductivity of CGS. Zinc in this research acts as an acceptor. The effect of zinc doping in CGS material is a decrease in the energy band gap and its band gap is smaller than undoped CGS. No n-type conductivity is produced. All these samples are p –type conductivity, confirmed by Hall Measurement [9]. N – type conductivity CGS only succeeds to fabricate using heavy co – doping Ge and Zn elements [11]. CGS always shows p – type conductivity, and can be explained using the doping pinning rule of $_{CGS}$. [12].

REFERENCES

[1] Saad, M., Riazi, H., Bucher, E. and Lux-Steiner, M. C. **"**$CuGaSe_2$ solar cells with 9.7% power conversation efficiency." Appl. Phys. A, 622 (1996): 181–185.

[2] Scheer, R. "Towards an electronic model for $Culn_{1-x}Ga_xSe_2$ solar cells." Thin Solid Films, 519.21 (2011) : 7472–7475.

[3] Puech, K., Zott, S., Leo, K., Ruckh, M. and Schock, H.W. "Determination of minority carrier lifetimes in $CuInSe_2$ thin films." Appl. Phys. Lett. 69, 22 (1996).

[4] Sathiabama Thiru, Masaki Asakawa, and Kazuki Honda. "Study of single crystal $CuInSe_2$ thin films and $CuGaSe_2/CuInSe_2$ single quantum well grown by molecular beam epitaxy." J. Crys. Growth, 425,03(2015): 203–206.

[5] Levchenko, S., Syrbu, N.N., Tezlevan, V. E., Arushanov, E., Merino, J. M. and Leon, M. "Exciton spectra and energy band structure of $CuGaSe_2$ single crystals." Appl. Phys. 41, no. 5 (2008) : 1–10.

[6] Subba Ramaiah Kodigala, Thin Films and Nanostructures $Cu(In_{1-x}Ga_x)Se_2$ based thin film solar cells. Elsevier, 2010. 195–255.

[7] Esser, N., Richte, W., Siebentrilt, S. and Ch. Lux – Steiner, M. "Compositional dependence of Raman scattering and photoluminescence emission in Cu_x Ga_y Se_2 thin films." Appl. Phys, 94 (2003): 4341.

[8] Yoshino, K., Sugiyama, M., Maruoka, D., Chichibu, S. F., Komaki, H. Umeda, K. and Ikari, T. "Photoluminescence spectra of $CuGaSe_2$ crystals." Physica B 302–303 (2001): 357-363.

[9] Sathiabama Thiru, Masaki Asakawa, and Kazuki Honda. "Study of Si doped and undoped Chalcopyrite $CuGaSe_2$ thin film." Appl. Physics A.113, (2015): 257 –261.

[10] Schon, J.H. "Extrinsic doping of $CuGaSe_2$ single crystal." Appl. Phys. 33 (2000): 286 –291.

[11] Schon, J.H., Riazi-Nejad, H., Kloc, C. H., Baumgartner, F. P. and Bucher, E. "Photoluminescence properties of doped- and undoped-$CuGaSe_2$ single crystals." Journal of Luminescence, 72 (1997) :118–120.

[12] Zhang, S.B., Wei, S. and Zunger, A. "A phenomenological model for systematization and prediction of doping limits in II – VI and I-III-VI2 compounds." Journal of applied physics 83, (1998).